Summer 2018

Synthesis and Characterization of Block Copolymers for Shear Force Responsive Materials and Sugar Conjugated Fluorescent Probes

Jacob Ryan Blankenship
Missouri State University, Blankenship335@live.missouristate.edu

SYNTHESIS AND CHARACTERIZATION OF BLOCK COPOLYMERS FOR

SHEAR FORCE RESPONSIVE MATERIALS AND SUGAR CONJUGATED

FLUORESCENT PROBES

A Masters Thesis

Presented to

The Graduate College of

Missouri State University

In Partial Fulfillment

Of the Requirements for the Degree

Master of Science, Chemistry

By

Jacob Ryan Blankenship

August 2018

SYNTHESIS AND CHARACTERIZATION OF SUGAR CONJUGATED

FLUORESCENT PROBES AND BLOCK COPOLYMERS FOR SHEAR FORCE

RESPONSIVE MATERIALS

Chemistry

Missouri State University, August, 2018

Master of Science

Jacob Ryan Blankenship

ABSTRACT

Herein, I present my work towards two goals: shear force-responsive materials and sugar-conjugated fluorescent probes for bacterial identification applications. The first work is on the development of stimuli-responsive polymers that allow for precise control over the release of encapsulated material. Stimuli-responsive polymers are becoming increasingly important in drug delivery and other applications. However there have been few reports on shear force-responsive micellar systems. I show the synthesis, and characterization by ^{1}H and ^{13}C NMR of four macro-chain transfer agents (macro-CTAs), one of which has not been previously reported. The resulting macro-CTAs were used in polymerization of vinyl acetate to yield amphiphilic diblock copolymers. The preliminary shear force-responsiveness of these polymers is evaluated using the FRET pair DiO and DiI as fluorescent reporters of location. The second work aims to outline the steps required for the synthesis of sugar-fluorophore conjugates, which contain one of three monosaccharides: glucose, mannose, and galactose covalently attached to one of three fluorophores: rhodamine B, fluorescein, and 6-hydroxycoumarin. The long-term goal of this work is to use the synthesized sugar-fluorophore conjugates for bacterial identification utilizing ratiometric analysis of carbohydrate binding/internalization rate.

KEYWORDS: RAFT polymerization, shear force-responsive, sugar, fluorophore, bacterial identification.

This abstract is approved as to form and content

_____
Keiichi Yoshimatsu, PhD
Chairperson, Advisory Committee
Missouri State University

SYNTHESIS AND CHARACTERIZATION OF SUGAR CONJUGATED

FLUORESCENT PROBES AND BLOCK COPOLYMERS FOR SHEAR FORCE

RESPONSIVE MATERIALS

By

Jacob Blankenship

A Masters Thesis
Submitted to the Graduate College
Of Missouri State University
In Partial Fulfillment of the Requirements
For the Degree of Master of Science, Chemistry

August, 2018

Approved:

_____

Keiichi Yoshimatsu, PhD

_____

Gautam Bhattacharyya, PhD

_____

Cyren Rico, PhD

_____

Kyoungtae Kim, PhD

_____

Julie Masterson, PhD: Dean, Graduate College

ACKNOWLEDGEMENTS

TABLE OF CONTENTS

LIST OF TABLES

LIST OF FIGURES

1. INTRODUCTION

In recent years, there has been great interest in stimuli-responsive polymers, including temperature, pH, photo-responsive, and multi-stimuli-responsive polymers.[1-5] Most often these are applied for drug delivery, but also hold promise in many other fields, including engineering. Despite the great interest on stimuli-responsive polymers, little has been reported on this system for the release of small-molecules in response to shear stress.

Shear force-responsive polymers could be of great use in biomedical applications and engineering.[6-11] A prime example is within an atherosclerotic artery (**Figure 1**).[6] The plaque build-up results in a size decrease of the blood vessel, and thus an increased flow in this area which results in an increased shear force felt on anything traveling through this size-restricted area. If, for example, a drug is encapsulated within a shear force-responsive micelle, this increase in shear force could trigger targeted drug release to this area.[6]
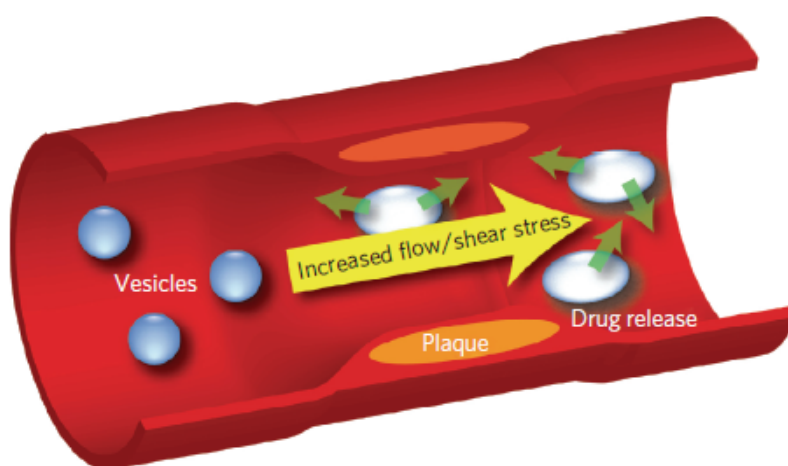
Figure 1. Increase of shear stress within an atherosclerotic artery. Reproduced from reference 6. Copyright 2012 Springer Nature.

Our goal is to synthesize amphiphilic block copolymers *via* Reversible Addition-Fragmentation chain Transfer (RAFT) polymerization and use these polymers in preparation of block copolymer micelles. The micellar structures are designed to break down and release the encapsulated material in response to a shear force of a certain magnitude. We propose the preparation of block copolymer micelles with an encapsulated hydrophobic Förster Resonance Energy Transfer (FRET) pair for use as fluorescent reporters (**Figure 2**). Because these block copolymers are amphiphilic, the polymer will self-assemble in solution with the hydrophilic block towards the bulk, aqueous solution and the hydrophobic tail blocks aggregated towards the center. This creates a hydrophobic area that can encapsulate the FRET pair.

Shear force

Figure 2. Micelle (blue) with encapsulated hydrophobic FRET pair (red). The hydrophobic material is released in response to a shear force.

The inclusion of a FRET pair will allow us to determine whether the hydrophobic fluorophores are inside the micelles, or whether the fluorophores are in bulk solution/precipitated. This serves as an indirect method of detecting whether the micelles have been broken or released the encapsulated material. Using a previously reported method [12,13], the donor fluorophore (3,3'-dioctadecyloxacarbocyanine perchlorate; **DiO**) will be excited at 425 nm. If present in the core of the micelle, the two fluorophores will

participate in FRET and the emission peak from the acceptor fluorophore (1,1'-dioctadecyl-3,3,3',3'-tetramethylindocarbocyanine perchlorate; **DiI**) should be present ~565 nm. If, however, there is no FRET peak, or a reduced FRET peak after introduction of a shear force, it is indicative of release of the FRET pair, and thus micelle breakage.

It might be possible to tune the magnitude of shear force required to break these block copolymer micelles, by keeping the hydrophobic block size constant, but increasing the length of the hydrophilic block. The hydrophobic block is the main driving force for micelle formation and the reason for one of the main stabilizing forces in a micellar system: the hydrophobic effect.[14] Our design is schematically depicted in **Figure 3**. By increasing the block length of the hydrophilic block, the micelle should feel a greater shear force due to the larger area occupied by the micelle. Shear force (stress) is directly proportional to the cross-sectional area of the material. Another driving force for the micelle breakage upon exposure to the shear force is associated with the solubility of the block copolymer itself. With longer hydrophilic blocks the block copolymer itself will be more soluble in the bulk aqueous solution and there will be a lower energy barrier. To our knowledge, there has been no utilization of this force-responsive nature in block copolymer micelles.
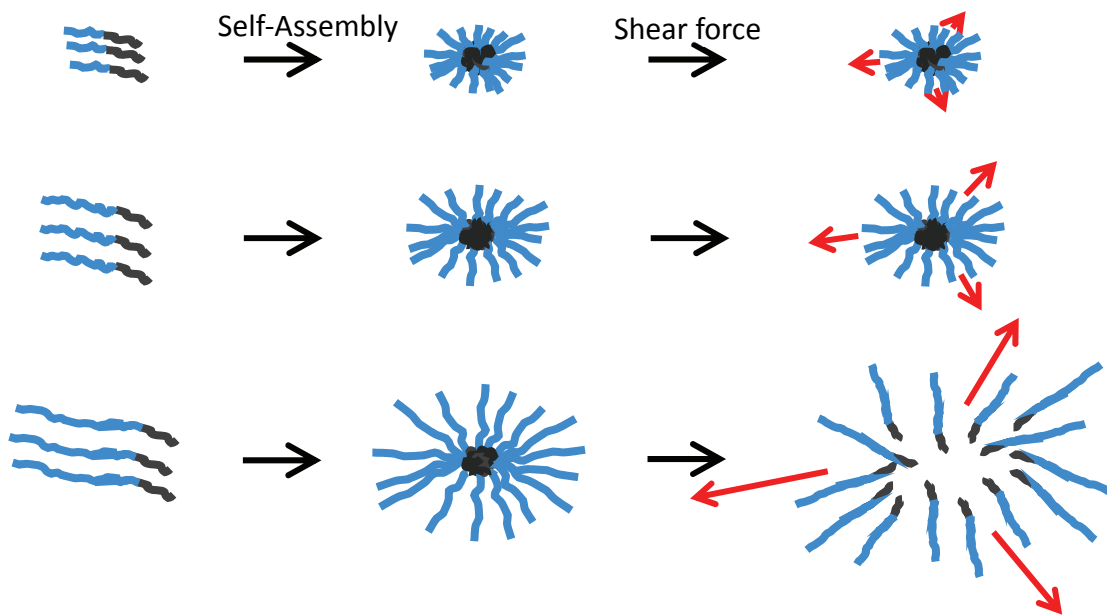
Figure 3. Schematic depiction of polymer design. Light blue segments represent hydrophilic blocks, whereas the dark blue represents hydrophobic blocks. Increasing the length of the hydrophilic block should increase the magnitude of shear force imparted to the micelle.

2. LITERATURE REVIEW

2.1 Shear Force-responsive Polymers

Larsen and Boydston recently reported an elastomeric polyurethane covalently linked to a benzyl furfuryl ether[15] (**Figure 4**). This resulted in scission of a covalent bond. However, to our knowledge, there have been no reports on force-responsive polymers that are designed to release encapsulated material upon exposure to force without chain scission.

Figure 4. Force-responsive polymer synthesized by Larsen and Boydston. Reproduced with permission from reference 15. Copyright American Chemical Society 2017.

2.2 Micelle Stability

There is limited literature available on the development of force-responsive micelles, though there have been related studies that are motivated by investigating micelle stability.[13] Micelle stability is critical in drug delivery because pre-mature release of encapsulated drugs results in loss of efficacy.[11] Kataoka and coworkers showed the loss of transfection efficiency in gene delivery by using poly(ethylene glycol)-*b*-poly(lysine) micelles carrying plasmid DNA (pDNA) under the shear stress. This is shown in **Figure 5**, where the increase in average rod length is a measure of degradation of micelle integrity. These shear stress values are in the range of those found in blood vessels.[8] Instead of utilizing this fact, the authors aimed to avoid this degradation of

micelle integrity to prevent premature release of the pDNA. To this aim, the polymers were covalently cross-linking by disulfide bonds to create a "cage" around the pDNA prevented loss of micelle integrity.
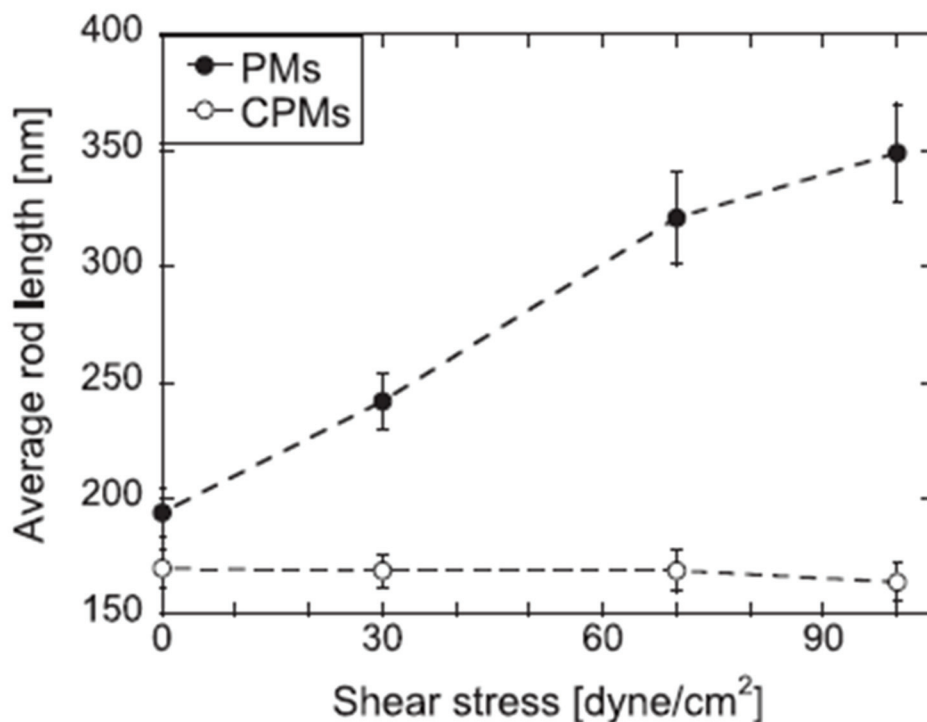
Figure 5. Degradation of micelles under shear-stress. PM: non-crosslinked micelles; CPM: crosslinked micelles utilizing disulfide bonds. The increase in average rod length is a measure of micelle degradation. Reproduced from reference 11 with permission from Elsevier.

2.3 Release of Encapsulated Cargo from Block Copolymer Micelles

Chen *et al.* have reported utilizing two hydrophobic fluorophores, which are Förster Resonance Energy Transfer (FRET) pairs, for trafficking of encapsulated drugs.[12,13] Since this FRET pair is hydrophobic, they are encapsulated in the center of the micelle in aqueous solution (**Figure 6**). These fluorophores are specifically chosen on two criteria: the fluorophores exhibit appropriate spectral overlap, that is, the emission

spectrum of one fluorophore (the donor) overlaps with the excitation spectrum of the other (the acceptor)[16] (**Figure 7**) and these fluorophores are hydrophobic enough to be encapsulated within the micelle in aqueous solution.
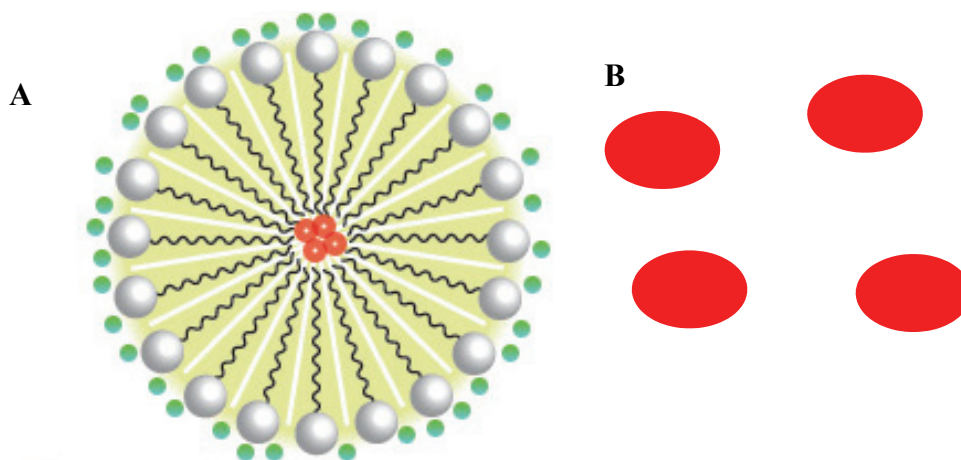
Figure 6. Illustration of micelle encapsulation. A. Micelle with encapsulated hydrophobic fluorophores. B. Hydrophobic fluorophores.
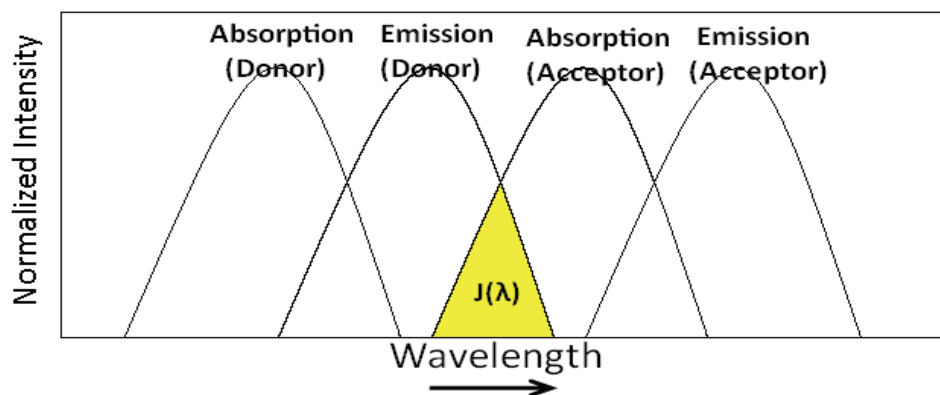
Figure 7: Schematic depiction of spectral overlap of a FRET pair. The yellow region represents the spectral overlap between the donor emission and acceptor absorption. Reference 16.

Because FRET is a highly distance dependent process, FRET will only take place if the two FRET pairs are in close proximity. In this system, that means it is possible to measure whether the micelles are intact. Chen *et al.* took advantage of this to measure the release of hydrophobic molecules from their model amphiphilic block copolymer,[12] monomethoxy poly(ethylene glycol)-*block*-poly(D,L-lactic acid). 3,3'-dioctadecyloxa-carbocyanine perchlorate (DiO) was used as the donor fluorophore and 1,1'-dioctadecyl-3,3,3',3'-tetramethylindocarbocyanine perchlorate (DiI) was used as the acceptor fluorophore (**Figure 8**). DiO was excited at 484 nm and the emission of DiI was measured from 490 nm to 590 nm using a confocal fluorescence microscope (**Figure 9**). The aim of their study was to determine whether whole micelles cross cell membranes, or just the encapsulated material in order to elucidate which pathway encapsulated drugs would utilize.
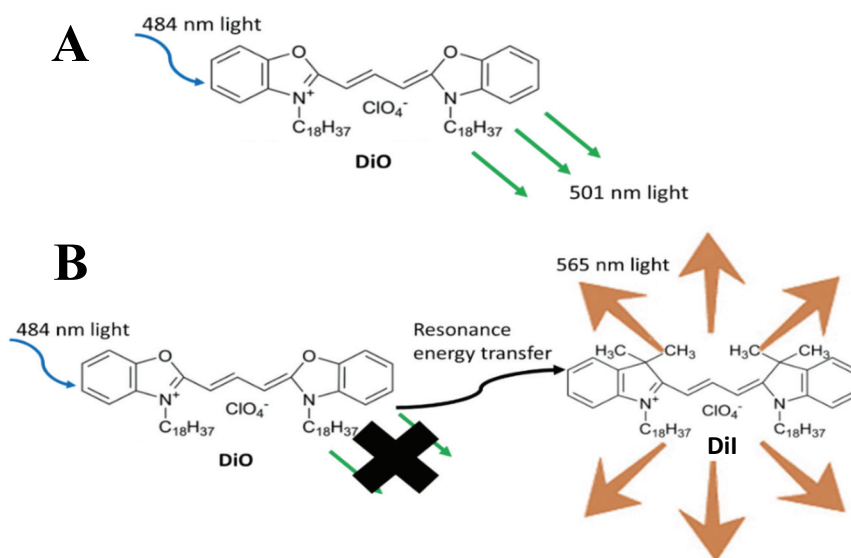
Figure 8. Förster resonance energy transfer between DiO and DiI. A: Excitation of DiO in absence of DiI. B: Excitation of DiO in close proximity to DiI. DiO: 3,3'-dioctadecyloxacarbocyanine perchlorate; DiI: 1,1'-dioctadecyl-3,3,3',3'-tetramethylindocarbocyanine perchlorate.
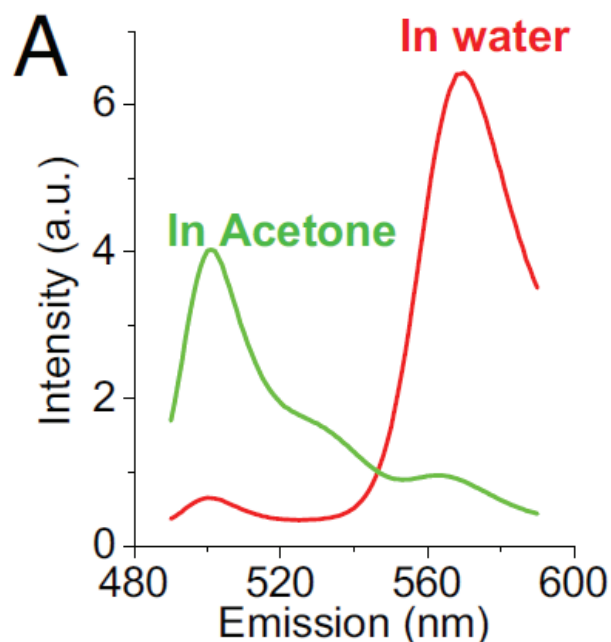
Figure 9. FRET signal from micelles containing DiO and DiI in water and acetone. The green line represents fluorescence from the donor DiO and the red line represents fluorescence from the acceptor, DiI. In acetone, no micelles are formed. Reproduced with permission from ref. 12. Copyright 2008 National Academy of Sciences.

2.4 RAFT Polymerization

Reversible Addition-Fragmentation Chain Transfer (RAFT) polymerization[17] is one of the reversible deactivation radical polymerizations (RDRP). RAFT polymerization has two main advantages over conventional radical polymerization: control of the chain end group, and a more uniform size distribution. Ideally during RAFT polymerization chain termination and irreversible chain transfer are absent due to the low concentration of reactive radicals, although this depends on the pairing of a chain transfer agent (**Figure 10**) and monomer.[17] As the name implies, the essence of this polymerization is that radicals on the main chains are able to react reversibly[18] (**Figure 11**) with use of a chain transfer agent, including xanthates (**Figure 10**).
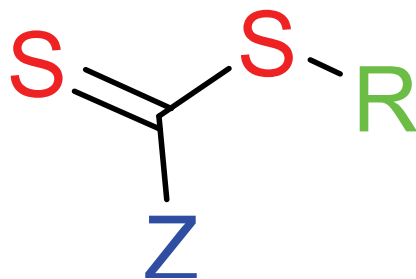
Figure 10. Schematic representation of a xanthate chain transfer agent. The R and Z groups variable chemical substituents that differ based on the monomer to be polymerized.

RAFT polymerization proceeds through the following steps (**Figure 11**):

2.4.1 Initiations. Radicals are first generated by decomposition of the initiator. This may either react with a monomer or the chain transfer agent.

2.4.2 Initialization/Pre-equilibrium. The growing polymer chain reacts with the chain transfer agent. This establishes the pre-equilibrium wherein either the growing polymer chain homolytically leaves or the R group of the chain transfer agent homolytically leaves. This is due to resonance stabilization of the radical and the relatively weak carbon-sulfur bond of the xanthate in the chain transfer agent.

2.4.3 Reinitiation. Once the R group homolytically leaves from the chain transfer agent, the radical at the end of the chain can react with monomers.

Initiation:
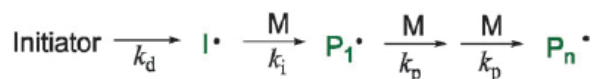
$$\text{Initiator} \xrightarrow{k_d} \text{I}\cdot \xrightarrow[k_i]{M} \text{P}_1\cdot \xrightarrow[k_p]{M} \xrightarrow[k_p]{M} \text{P}_n\cdot$$

Initialization/Pre-equilibrium:

1   **3**   **2**

Reinitiation:

$$\text{R}\cdot \xrightarrow[k_{iR}]{M} \text{P}_1\cdot \xrightarrow[k_p]{M} \xrightarrow[k_p]{M} \text{P}_m\cdot$$

Main equilibrium:

2   **4**   **2**

Termination:

$$\text{P}_n\cdot + \text{P}_m\cdot \xrightarrow{k_t} \text{dead polymer}$$
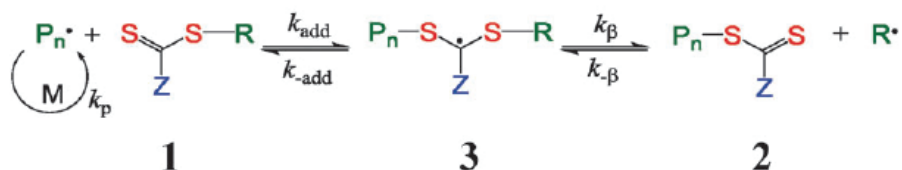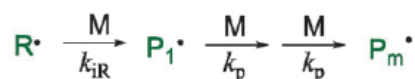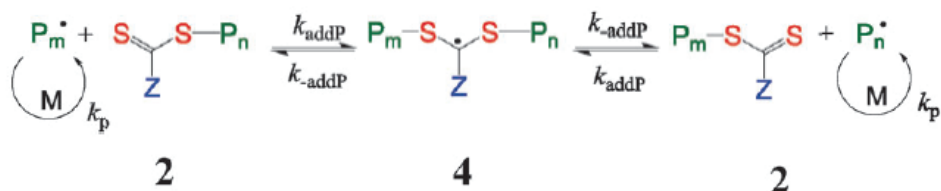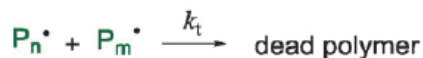
Figure 11. General mechanism of RAFT polymerization. Reproduced from reference 18 Copyright 2013 Royal Society of Chemistry. Abbreviations, M: monomer, P: polymer, k: rate constant, R and Z: variable groups dependent on CTA.

2.4.4 Main Equilibrium. The radical can also react with the chain transfer agent. This establishes the main equilibrium, where the reaction will spend most of the time. In contrast to traditional polymerizations, most of the time growing chains are in a dormant state (2 in **Figure 8**) and are unable to participate in chain propagation or termination. Importantly, this allows for a more uniform size distribution of synthesized polymers due to the introduction of an equilibrium state, yielding monodisperse samples when the

correct chain transfer agent-monomer pair are chosen.[17-19] Propagation may proceed after either polymer chain is homolytically cleaved.

2.5 Choice of a Chain Transfer Agent (CTA)

The choice of chain transfer agent is critical in order to achieve good control of molecular weights. R and Z groups must be chosen so that $k_{add} \gg k_p$, and $k_\beta \gg k_p$,[17-19] in other words, the rate that a growing polymer chain, that is not attached to the chain transfer agent, propagates should be slower than the rate at which equilibrium is established, and the homolytic cleavage of the "R" group on the chain transfer agent should be greater than the propagation rate of the growing homopolymer (propagation of monomers without use of the CTA). As mentioned above, the R group of the chain transfer agent must be a good homolytic leaving group with respect to P_n radical.[18,19] There have been general guidelines established in literature (**Figure 12**).
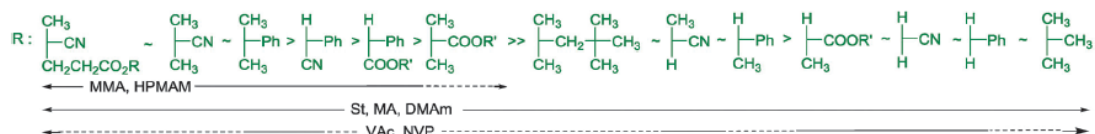
Figure 12. General guidelines for selection of chain transfer agent R group. Dashed lines indicate partial control over polymerization, solid line indicates good control. Abbreviations: MMA: methyl methacrylate, HPMAM: *N*-(2-hydroxypropyl) methacrylamide, St: styrene, DMAm: *N,N*-dimethylacrylamide, VAc: vinyl acetate, NVP: *N*-vinylpyrrolidone. Reproduced with permission from reference 18. Copyright 2018 Royal Society of Chemistry.

Similarly, the choice of "Z" group is also vital. The Z group influences the reactivity of the thiocarbonyl group towards radical addition and the rate of fragmentation

of the RAFT intermediate radical[18] (3 and 4 in **Figure 8**). General guidelines for the

choice of Z group are shown in **Figure 13**.[18]
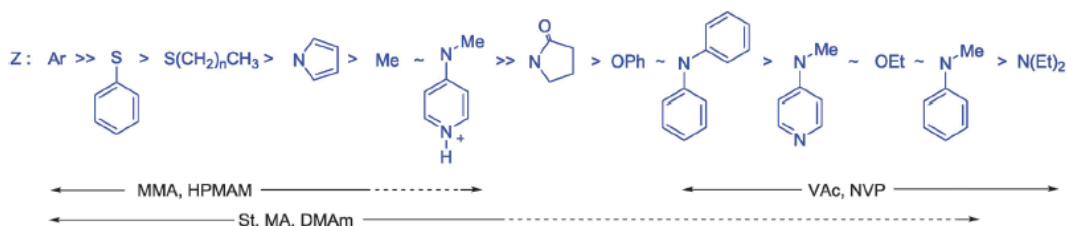
Figure 13. General guidelines for selection of chain transfer agent Z group. Dashed lines indicate partial control over polymerization, solid line indicates good control. Abbreviations: MMA: methyl methacrylate, HPMAM: *N*-(2-hydroxypropyl) methacrylamide, St: styrene, DMAm: *N,N*-dimethylacrylamide, VAc: vinyl acetate, NVP: *N*-vinylpyrrolidone. Reproduced with permission from reference 18. Copyright 2018 Royal Society of Chemistry.

2.6 Macro Chain Transfer Agent (macro-CTA)

Recently, there have been some reports on using a macro-chain transfer agent,

CTAs that are polymers themselves *e.g.* contains PEG repeat units for an R group

(**Figure 14**).[20-22] Macro-CTAs are gaining popularity as a way to synthesize block

copolymers. Popular monomers for use with macro-CTAs include: *N*-

isopropylacrylamide (NIPAM), acrylamide, *N*-vinylpyrrolidone (NVP), styrene, and

methyl methacrylate (MAM).[20,21,23] However, there have been very few reports using a

macro-CTA with vinyl acetate (VAc). In fact, to our knowledge, there is only two other

utilizing a PEG derived macro-CTA for polymerization with VAc. In one study, very

little data was presented,[20] and in the other, an emulsion polymerization was used and

provided very poor control with PDIs (polydispersity indexes) ~2, as determined by GPC

(gel permeation chromatography).[24]
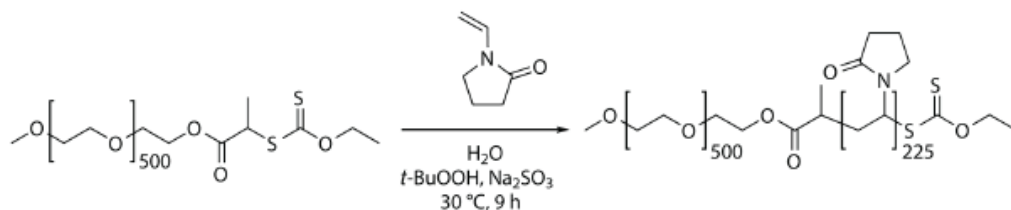
Figure 14. Macro-CTA used in the polymerization of *N*-vinylpyrrolidone. Reprinted with permission from reference 21. Copyright 2016 American Chemical Society.

2.7 Vinyl Acetate (VAc)

Polyvinyl acetate (PVAc) is a hydrophobic and non-toxic polymer that is approved by the Food and Drug Administration (FDA) for use in food packaging.[24,25] Furthermore, VAc has many uses in industry ranging from applications in adhesives, paints, concrete additives, to pharmaceuticals.[26] Despite these uses, VAc is not used often in RAFT polymerization utilizing a macro-CTA, and systematic studies of VAc in RAFT polymerizations are not common.[24,26] Despite this, our inspiration to use VAc as our hydrophobic block comes from the commercially available and FDA approved graft copolymer, Soluplus® (**Figure 15**).[27] We omit vinyl caprolactam from our target copolymers due to the thermo-responsive nature.
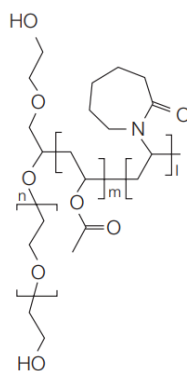
Figure 15. Structure of Soluplus®. The brackets with m, n, and i represent repeat units of 13% PEG 6000, 57% vinyl caprolactam, and 30% vinyl acetate. $M_n = 90,000 - 140,000$. Reference 27

14

3. EXPERIMENTAL

3.1 Chemicals

The following chemicals were used in this work:

1-Ethyl-3-(3-dimethylaminopropyl)carbodiimide hydrochloride (EDC) (Creo Salus), 1892-57-5
2-bromopropionyl bromide, > 98.0% (TCI chemicals), 563-76-8
4-dimethylaminopyridine (DMAP), 99% (Acros Organics), 1122-58-3
6-hydroxycoumarin, 98% (Acros Organics), 6093-68-1
Acetone, ACS grade (Fisher Chemical), 67-64-1
Ammonium Chloride (Fisher Chemical), 12125-02-9
Anhydrous diethyl ether, BHT stab., ACS grade (Fisher Chemical), 60-29-7
Basic alumina, 80-200 mesh (Fisher Scientific), 1344-28-1
Bromoacetyl bromide, > 98.0% (TCI chemicals), 598-21-0
Chloroform-*d*, 99.8+ atom % D, with 0.03 v/v % TMS (Acros Organics), 865-49-6
Dichloromethane (DCM), HPLC grade (Fisher Chemical), 75-09-2
DiI (1,1'-Di-*n*-octadecyl-3,3,3',3'-tetramethylindocarbocyanine perchlorate), 97% (Alfa Aesar), 41085-99-8
DiO (3,3'-Dioctadecyloxacarbocyanine perchlorate) (Marker Gene Technologies, Inc.), 34215-57-1
Ethyl acetate, ACS grade (Fisher Chemical), 141-78-6
Fluorescein, sodium salt (Sigma Aldrich), 518-47-8
Hexanes, HPLC grade (Fisher Chemical), 73513-42-5
Magnesium sulfate, anhydrous (Chem-Impex Int'l, Inc.), 7487-88-9
Methanol, HPLC grade (Fisher Chemical), 67-56-1
N,*N*-Dimethylforamide (DMF), ACS grade, (Fisher Chemical), 68-12-2
PEG(5000)-*b*-PLA(5000) (Polysciences, Inc.), 24389-0.5
Poly(ethylene glycol) monomethyl ether (mPEG) 2000 (Sigma Aldrich), 9004-74-4
Poly(ethylene glycol) monomethyl ether (mPEG) 4000 (TCI Chemicals), 9004-74-4
Poly(ethylene glycol) monomethyl ether (mPEG) 5000 (Sigma Aldrich), 9004-74-4
Potassium Carbonate, anhydrous (Fisher Chemical), 584-08-7
Potassium iodide, anhydrous (Sigma Aldrich), 7681-11-0
Potassium *O*-ethyl xanthate, 97 +% (Acros Organics), 140-89-6
Propargyl alcohol, 99% (Alfa Aesar), 107-19-7
p-toluenesulfonyl chloride (TsCl), 99 +% (Acros Organics), 98-59-9
Pyridine (JT Baker Chemicals), 110-86-1
Rhodamine B (Allied Chemical), 81-88-9
Silver nitrate, 99.9% (Beantown Chemical), 7761-88-8
Sodium bicarbonate (Fisher Chemical), 144-55-8
Sodium hydroxide, pellets, anhydrous > 98% (1310-73-2)
Sulfuric acid, concentrate (Fisher chemical), 7664-93-9
Tetrahydrofuran, 99%, stab. with 250 - 350 ppm BHT (Alfa Aesar), 14044-65-6
Triethylamine (VWR), 121-44-8

Triethylene glycol, > 99.0% (TCI Chemicals), 112-27-6
Vinyl acetate (VAc), > 99.0 %, stab. with HQ (TCI Chemicals), 108-05-4

3.2 Instrumentation

3.2.1 Nuclear Magnetic Resonance (NMR). ^{1}H NMR spectra were recorded on

Varian 400 MHz Unity INOVA spectrometer using tetramethylsilane (TMS) as the

internal standard. ACD labs 12.0 NMR processing software was used for ^{1}H and [13]C

NMR data analysis. All NMR studies were conducted at 25 °C, spinning at 20 Hz. The

parameters of each study, unless otherwise noted, were as follows: 5 second acquisition

time, 5 second relaxation time with 45 ° pulse angle and 65 scans for ^{1}H NMR. ^{1}H NMR

spectra were corrected by the deuterated solvent peak rather than by TMS, setting $CDCl_3$

to 7.27 ppm, and DMSO-d_6 to 2.50 ppm. ^{13}C NMR spectra were corrected by the

deuterated solvent peak, setting $CDCl_3$ to 77.00 ppm and DMSO-d_6 to 39.51 ppm.

3.2.2 Fluorimetry. All fluorescence spectra were recorded using a Photon

Technology International, Inc. fluorimeter. Instrumental settings were as follows:

excitation slit width: 8 nm, emission slit width: 10 nm, excitation wavelength: 425 nm,

emission scan from 450 nm – 650 nm, recording every 1 nm. All fluorescence studies

were conducted using a 3 mL quartz cuvette with a 1 cm path length. All fluorescence

spectra are presented after subtracting a blank with solvent alone.

3.3 Overview of Polymer Synthetic Route

3.3.1 Synthetic Route for Methyl Substituted Macro-CTAs. These macro-

CTAs are synthesized using a modified protocol from Zhao *et al.* [23] (**Figure 16**). First,

poly(ethylene glycol) monomethyl ether (n= 45, 90, or 112 for M_n = 2,000 g/mol , 4,000

g/mol, or 5,000 g/mol, respectively) is reacted with 2-bromopropionyl bromide in DCM in the presence of pyridine to yield the brominated mPEG as an intermediate. Next, this intermediate is reacted with potassium O-ethyl xanthate in DCM in the presence of pyridine to yield our methyl substituted macro-CTA, S-2-(monomethoxy poly(ethylene glycol)propionate)-(O-ethyl xanthate).
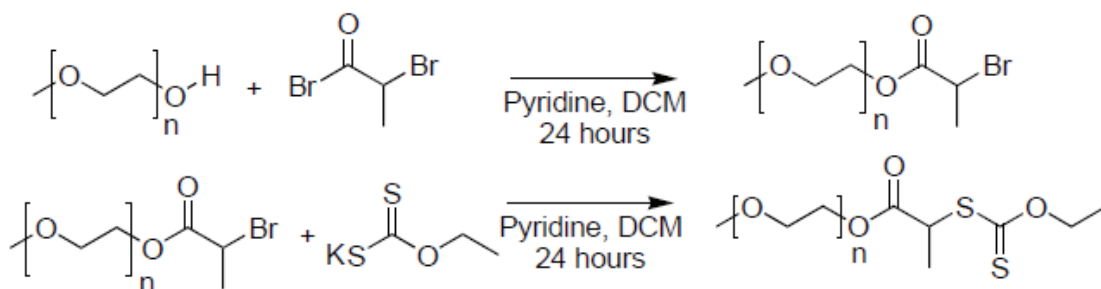
Figure 16. Synthetic route for methyl substituted Macro-CTA, S-2-(monomethoxy poly(ethylene glycol)propionate)-(O-ethyl xanthate).

3.3.2 Synthetic Route for Unsubstituted Macro-CTAs. The macro-CTAs are synthesized using a modified protocol from Zhao *et al.* [23] (**Figure 17**). First, poly(ethylene glycol) monomethyl ether (n = 45, 90, or 112 for M_n = 2,000 g/mol , 4,000 g/mol, or 5,000 g/mol, respectively) is reacted with bromoacetyl bromide in DCM in the presence of pyridine to yield the brominated mPEG as an intermediate. Next, this intermediate is reacted with potassium O-ethyl xanthate in DCM in the presence of pyridine to yield our macro-CTA, S-(monomethoxy poly(ethylene glycol)acetate)-(O-ethyl xanthate).
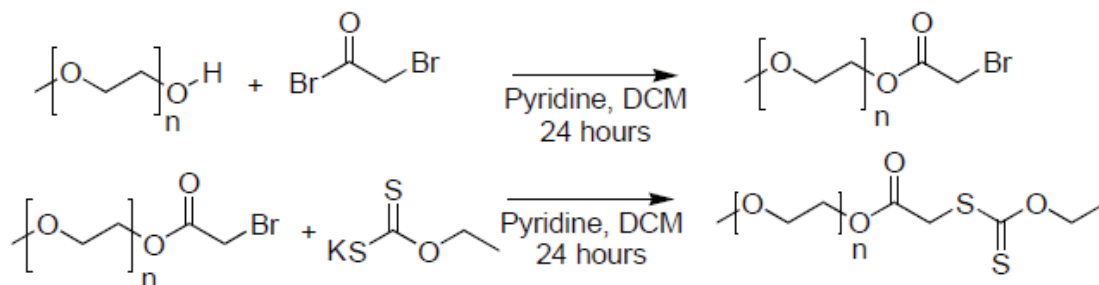
Figure 17. Synthetic route for unsubstituted macro-CTA *S*-(monomethoxy poly(ethylene glycol)acetate)-(*O*-ethyl xanthate).

3.3.3 RAFT Polymerization of Vinyl Acetate with Macro-CTAs. The previously synthesized macro-CTA was reacted with inhibitor-free vinyl acetate in inhibitor-free THF containing AIBN as the initiator ~60 °C under a nitrogen atmosphere (**Figure 18**). The polymerization was stopped by removal from the heat source and exposure to oxygen.
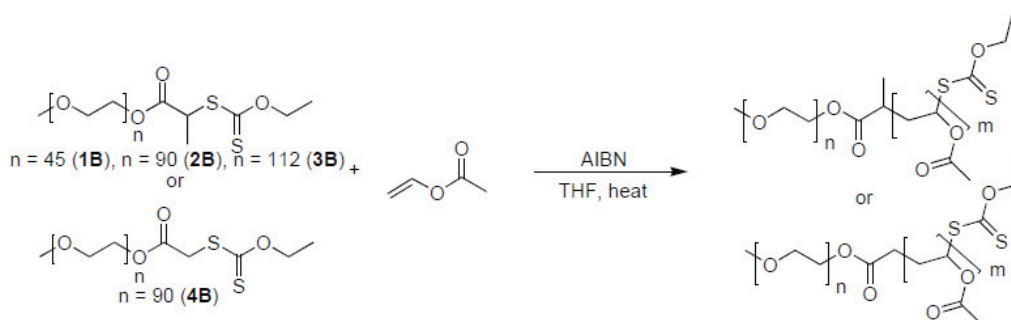
Figure 18. RAFT polymerization of vinyl acetate with macro-CTAs.

3.4 Synthesis of Macro-Chain Transfer Agents

3.4.1 Monomethoxy Poly(ethylene glycol) 2,000 2-bromoethyl Ester (1A). A protocol from *Zhao et al.*[23] was adapted and modified for our synthesis. Generally, 3.0

grams of poly(ethylene glycol) (M_n = 2,000 g/mol) were dissolved in 15 mL of DCM in a 25 mL round bottom flask with a stir bar, followed by addition of 0.300 mL of pyridine. After stirring on an ice bath for 5 minutes, 0.400 mL of 2-bromopropionyl bromide was added dropwise through a rubber septum using a nitrogen purged syringe. After addition of 2-bromo propionyl bromide the reaction was stirred for an additional 5 minutes on an ice bath. The ice bath was removed and the reaction was left to warm to room temperature with stirring. The reaction was wrapped with aluminum foil to protect from light and reacted at room temperature for 24 hours. A white precipitate was removed by filtration and the filtrate was diluted with 45 mL of DCM. Followed by dilution with DCM, the filtrate was washed with saturated ammonium chloride (8 mL x 4), saturated $NaHCO_3$ (8 mL x 4), and deionized water (8 mL). The organic layer was then dried over anhydrous magnesium sulfate and then precipitated dropwise into 300 mL of cold diethyl ether. The product was recovered by vacuum filtration through a Gooch funnel and dried to yield a white solid (2.6 g, 80.1 % yield): ^{1}H NMR (400 MHz, CDCl$_3$,): δ 4.36 (q, J = 8 Hz, 1H, **CH**), 4.28 (m, 2H, **CH$_2$**OC(O)), 3.60 (s), 3.41-3.79 (m, **CH$_2$CH$_2$**O- of PEG backbone), 3.34 (s, 3H, -O**CH$_3$**), 1.79 (d, J = 8 Hz, 3H, **CH$_3$**). ^{13}C NMR (100 MHz, CDCl$_3$): δ 170.05, 68.59-71.77, 64.86, 58.86, 39.76, 21.48. (**Appendix A-1**)

3.4.2 Monomethoxy Poly(ethylene glycol) 4,000 2-bromoethyl Ester (2A). A modified protocol from Zhao *et al.*[23] was used. 15.0318 grams of poly (ethylene glycol) (M_n = 4,000 g/mol) were dissolved in a 100 mL round bottom flask in 37.5 mL of DCM with a stir bar, followed by addition of 0.750 mL of pyridine. After stirring on an ice bath for 5 minutes, 0.900 mL of 2-bromopropionyl bromide was added dropwise through a rubber septum using a nitrogen purged syringe. After addition of 2-bromopropionyl

bromide was complete the reaction was stirred for an additional 5 minutes on an ice bath and then let warm to room temperature with stirring. The reaction was wrapped with aluminum foil to protect from light and reacted at room temperature for 24 hours. A white precipitate was removed by filtration and the filtrate was diluted with 120 mL of DCM. Followed by dilution with DCM, the filtrate was washed with saturated ammonium chloride (20 mL x 4), saturated $NaHCO_3$ (20 mL x 4), and 20 mL of deionized water. The organic layer was then dried over anhydrous magnesium sulfate and crude product was recovered after removal of the solvent under vacuum to yield and off-white solid. ^1H NMR (400 MHz, CDCl$_3$): δ 4.23 (q, $J = 8$ Hz, 1H, **CH**), 4.13 (m, 2H, **CH$_2$**OC(O)), 3.45 (s), 3.26-3.64 (m, **CH$_2$CH$_2$**O- of PEG backbone), 3.18 (s, 3H, -OC**H$_3$**), 1.63 (d, $J = $ 8 Hz, 3H, C**H$_3$**) (**Appendix A-2**). ^{13}C NMR (100 MHz, CDCl$_3$): δ 169.45, 71.29, 69.94, 68.09, 58.36, 39.35, 21.04 (**Appendix A-3**).

3.4.3 Monomethoxy Poly(ethylene glycol) 5,000 2-bromoethyl Ester (3A). A modified protocol from Zhao *et al.*[23] was used. 4.9865 grams of poly(ethylene glycol) (M_n = 5,000 g/mol) were dissolved in a 25 mL round bottom flask in 10 mL of DCM with a stir bar, followed by addition of 0.300 mL of pyridine. After stirring on an ice bath for 5 minutes, 0.300 mL of 2-bromopropionyl bromide was added dropwise through a rubber septum using a nitrogen purged syringe. After addition of 2-bromopropionyl bromide was complete the reaction was stirred for an additional 5 minutes on an ice bath and then let warm to room temperature with stirring. The reaction was wrapped with aluminum foil to protect from light and reacted at room temperature for 24 hours. A white precipitate was removed by filtration and the filtrate was diluted with 40 mL of DCM. Followed by dilution with DCM, the filtrate was washed with saturated ammonium chloride (5 mL x

4), saturated NaHCO$_3$ (5 mL x 4), and 5 mL of deionized water. The organic layer was then dried over anhydrous magnesium sulfate and then precipitated into 500 mL of cold diethyl ether. The filtrate was recovered by vacuum filtration through a Gooch funnel, collected and dried to yield a white solid (3.3936 g, 66.3 % yield): ^{1}H NMR (400 MHz, CDCl$_3$): δ 4.24 (q, J = 4 Hz, 1H, C**H**), 4.14 (m, 2H, C**H$_2$**OC(O)), 3.47 (s), 3.28-3.66 (m, C**H$_2$**C**H$_2$**O- of PEG backbone), 3.20 (s, 3H, -OC**H$_3$**), 1.66 (d, J = 4 Hz, C**H$_3$**) (**Appendix A-4**). ^{13}C NMR (100 MHz, CDCl$_3$): δ 169.54, 69.78-71.36, 64.43, 58.42, 39.41, 21.11 (**Appendix A-5**).

3.4.4 Monomethoxy Poly(ethylene glycol) 4,000 Bromomethyl Ester (4A). A modified protocol from Zhao *et al.*[23] was used. 15.0046 grams of poly (ethylene glycol) (M_n = 4,000 g/mol) were dissolved in a 100 mL round bottom flask in 37.5 mL of DCM with a stir bar, followed by addition of 0.750 mL of pyridine. After stirring on an ice bath for 5 minutes, 0.900 mL of 2-bromo acetyl bromide was added dropwise through a rubber septum using a nitrogen purged syringe. After addition of bromoacetyl bromide was complete the reaction was stirred for an additional 5 minutes on an ice bath and then let warm to room temperature with stirring. The reaction was wrapped with aluminum foil to protect from light and reacted at room temperature for 24 hours. A white precipitate was removed by filtration. The filtrate was precipitated dropwise into 500 mL of cold diethyl ether and collected by vacuum filtration through a Gooch funnel. The crude product was recovered after removal of the solvent under vacuum to yield and off-white solid. ^{1}H NMR (400 MHz, CDCl$_3$): δ 4.31 (m, 2H, C**H$_2$**OC(O)), 3.86 (s, 2H, C**H$_2$**), 3.62 (s), 3.43-3.84 (m, C**H$_2$**C**H$_2$**O- of PEG backbone), 3.36 (s, 3H, -OC**H$_3$**).

3.4.5 *S*-2-(Monomethoxy Poly(ethylene glycol) 2,000 Propionate)-(*O*-ethyl Xanthate) (1B). A modified protocol from Zhao *et al.*[23] was used. 0.4205 grams of **1A** was dissolved in a 15 mL tube in 3 mL of DCM with a stir bar, followed by addition of 0.840 mL of pyridine. After stirring until completely dissolved, 0.1019 grams of potassium *O*-ethyl xanthate was added portionwise. The reaction was covered from light and reacted with stirring for 24 hours. The reaction mixture was then filtered to remove a yellow precipitate and 14 mL of DCM was added to the filtrate. The filtrate was washed with saturated ammonium chloride (4 mL x 4), saturated sodium bicarbonate (4 mL x 4), and 5 mL deionized water. The organic layer was then dried over anhydrous magnesium sulfate and then precipitated into 50 mL of cold diethyl ether and collected by vacuum filtration through a Gooch funnel. The pure product was obtained after removal of solvent under vacuum (0.2017 g, 47.0 % yield): ^{1}H NMR (400 MHz, CDCl$_3$): δ 4.63 (q, 2H, $J = 8$ Hz, SC(S)OC**H**$_2$CH$_3$), 4.41 (q, 1H, $J = 8$ Hz, C**H**CH3), 4.29 (m, 2H, C**H**$_2$OC(O)) 3.63 (s), 3.44-3.82 (m, C**H**$_2$C**H**$_2$O- of PEG backbone), 3.37 (s, 3H, -OC**H**$_3$), 1.57 (d, $J = 2$H, 8 Hz, CHC**H**3), 1.41 (t, 3H, $J = 8$ Hz, SC(S)OCH2C**H**3) (**Appendix A-6**).

3.4.6 *S*-2-(Monomethoxy Poly(ethylene glycol) 4,000 Propionate)-(*O*-ethyl Xanthate) (2B). A modified protocol from Zhao *et al.*[23] was used. The crude product from **2A** was dissolved in a 200 mL round bottom flask in 55.8 mL of DCM with a stir bar, followed by addition of 16.0 mL of pyridine. After stirring until completely dissolved, 1.8357 grams of potassium *O*-ethyl xanthate was added portionwise. The reaction was covered from light and reacted with stirring for 21 hours. The reaction mixture was then filtered to remove a yellow precipitate and 120 mL of DCM was added

to the filtrate. The filtrate was washed with 3 x 50 mL saturated ammonium chloride, 3 x 50 mL saturated sodium bicarbonate, and 50 mL deionized water. The organic layer was then dried over anhydrous magnesium sulfate and then dried under vacuum to obtain a white solid. (13.4 g 85.2 % yield): ^{1}H NMR (400 MHz, CDCl$_3$): δ 4.60 (q, 2H, J = 8 Hz, SC(S)OC**H**$_2$CH$_3$), 4.38 (q, 1H, J = 8 Hz, C**H**CH3), 4.26 (m, 2H, C**H**$_2$OC(O)) 3.60 (s), 3.44-3.79 (m, C**H**$_2$C**H**$_2$O- of PEG backbone), 3.34 (s, 3H, -OC**H**$_3$), 1.55 (d, 2H, J = 8 Hz, CHC**H**3), 1.38 (t, 3H, J = 8 Hz, SC(S)OCH2C**H**3). ^{13}C NMR (100 MHz, CDCl$_3$): δ 211.78, 171.19, 109.91, 68.71-71.77, 64.64, 58.87, 46.93, 16.73, 13.53 (**Appendix A-8**).

3.4.7 *S*-2-(Monomethoxy Poly(ethylene glycol) 5,000 Propionate)-(*O*-ethyl Xanthate) (3B). A modified protocol from Zhao *et al.*[23] was used. 0.5093 grams of **3A** was dissolved in a 15 mL tube in 1.5 mL of DCM with a stir bar, followed by addition of 0.420 mL of pyridine. After stirring until completely dissolved, 0.0515 grams of potassium *O*-ethyl xanthate was added. The reaction was wrapped in aluminum foil to protect from light and reacted with stirring for 24 hours. The reaction mixture was then filtered to remove a yellow precipitate and 14 mL of DCM was added to the filtrate. The filtrate was washed with saturated ammonium chloride (4 mL x 4), saturated sodium bicarbonate (4 mL x 4), and 5 mL deionized water. The organic layer was then dried over anhydrous magnesium sulfate and then precipitated into 50 mL of cold diethyl ether and collected by vacuum filtration through a Gooch funnel. The pure product was obtained as a white solid after removal of solvent under vacuum (0.3864 g, 73.3 % yield): ^{1}H NMR (400 MHz, CDCl$_3$): δ 4.56 (q, 2H, J = 8 Hz, SC(S)OC**H**$_2$CH$_3$), 4.33 (q, 1H, J = 4 Hz, C**H**CH3), 3.57 (s), 3.39-3.3.76 (m, C**H**$_2$C**H**$_2$O- of PEG backbone), 3.30 (s, 3H, -OC**H**$_3$), 1.51 (d, 2H, J = 4 Hz, CHC**H**3), 1.34 (t, 3H, J = 8 Hz, SC(S)OCH2C**H**3) (**Appendix A-**

7). ^{13}C NMR (100 MHz, CDCl$_3$): δ 211.33, 170.76, 68.29-71.35, 58.44, 46.49, 31.54, 16.31, 13.11 (**Appendix A-8**).

3.4.8 *S*-(Monomethoxy Poly(ethylene glycol) 4,000 Acetate)-(*O*-ethyl Xanthate) (4B). A modified protocol from Zhao *et al.*[23] was used. The crude product from **4A** was dissolved in a 200 mL round bottom flask in 55.8 mL of dichloromethane with a stir bar, followed by addition of 16.0 mL of pyridine. After stirring until completely dissolved, 1.7872 grams of potassium *O*-ethyl xanthate was added portionwise. The reaction was wrapped in aluminum foil to protect from light and reacted with stirring for 25 hours. The reaction mixture was then filtered to remove a yellow precipitate and 120 mL of DCM was added to the filtrate. The filtrate was washed with saturated ammonium chloride (50 mL x 3), saturated sodium bicarbonate (50 mL x 3), and 50 mL deionized water. The organic layer was then dried over anhydrous magnesium sulfate and then precipitated dropwise into 500 mL of cold diethyl ether and collected by vacuum filtration through a Gooch funnel. Pure product was obtained as a yellow solid after drying under vacuum (7.5811 g, 68.3 % yield over two steps): ^{1}H NMR (400 MHz, CDCl$_3$): δ 4.60 (q, 2H, *J* = 8 Hz, SC(S)OC**H**$_2$CH$_3$), 4.27 (m, 2H, C**H**$_2$OC(O)), 3.92 (s, 2H, C**H**$_2$), 3.60 (s), 3.41-3.79 (m, C**H**$_2$C**H**$_2$O- of PEG backbone), 3.33 (s, 3H, -OC**H**$_3$), 1.38 (t, 3H, *J* = 8 Hz, SC(S)OCH2C**H**3).

3.5 RAFT Polymerization of Vinyl Acetate (VAc) with Macro-Chain Transfer Agents (macro-CTA)

THF (stabilized with BHT) and VAc (stabilized with HQ) were passed through a short plug of basic alumina immediately prior to use. In some cases, after removal of the

inhibitor *via* basic alumina, the VAc and THF were stored in the refrigerator at 4 °C, wrapped in aluminum foil in a 20 mL scintillation vial for up to 3 days before use. Generally, the previously synthesized macro-CTA was added to a 15 mL pear-shaped flask with a spin vane. Then, inhibitor-free THF was added as solvent followed by addition of recrystallized AIBN that was previously dissolved in THF. Finally, inhibitor-free vinyl acetate was added. Four freeze-pump-thaw cycles were performed on the reaction mixture to remove any oxygen dissolved in solution. After the final freeze-pump-thaw cycle, the vessel was filled with nitrogen gas and reacted on an oil bath to initiate the polymerization. After the reaction period, the polymerization was stopped by removal from heat. While the reaction was still warm, it was precipitated dropwise into 25 mL of hexanes, followed by centrifugation at 4,696 x g for 5 minutes, and then removal of the supernatant. The resulting viscous oil was then dried under vacuum for several hours to yield a slightly yellow solid. Degree of polymerization for each copolymer was calculated from each ^{1}H NMR by setting the PEG backbone, plus methoxy group integration value to 181 for macro-CTA **1B** reactions, and 361 for macro-CTAs **2B** and **4B** as reference integration values. It is important to note, that the CH_2 group closest to the ester linkage in the PEG backbone was not included in this, as it is shifted lower field than the other PEG protons. Next, the CH_2 and CH_3 groups from the VAc repeat units were integrated. This integrated value (with the PEG backbone, plus methoxy group set as reference) was divided by 5 to determine the number of repeat units of VAc, or the degree of polymerization.

3.6 Freeze-pump-Thaw Cycles

Freeze-pump-thaw cycles were performed by equipping the reaction vessel with a

vacuum stopcock with all ground glass joints greased with vacuum grease to prevent any

leaks. The stopcock was closed and the reaction vessel submerged in liquid nitrogen.

After completely freezing, the vessel was removed from liquid nitrogen and a vacuum

line was connected to the vacuum stopcock with the vacuum on. The stopcock was

opened and the vessel evacuated under vacuum. The vacuum stopcock was then closed

while the vacuum was still running. The vacuum line was removed and the reaction

mixture was let warm at room temperature until the solvent had completely melted and

was no longer cloudy. This procedure was repeated three more times. After the last cycle,

the vessel was filled with nitrogen gas.

3.7 Recrystallization of AIBN

To a 20 mL scintillation vial equipped with a mini stir bar, 0.3482 g of AIBN was

added, followed by addition of 2 mL of methanol at room temperature. The AIBN

mixture was then placed into a 45 °C water bath and ~2.5 mL of 40 °C methanol was

added, which completely dissolved the AIBN. The AIBN solution was then let cool to

room temperature to recrystallize. The resulting sharp, white crystals were then collected

via vacuum filtration and dried under vacuum. The recrystallized AIBN was stored in a

20 mL scintillation vial wrapped with aluminum foil in the freezer at -20 °C until use.

3.8 Preparation of FRET Micelles

DiI (1,1'-dioctadecyl-3,3,3',3'-tetramethylindocarbocyanine perchlorate) and DiO (3,3'-dioctadecyloxacarbocyanine perchlorate) were dissolved in methanol in separate 1.5 mL microcentrifuge tubes to prepare 1.9 mg/mL and 1.0 mg/mL solutions, respectively. FRET micelles were prepared using a modified protocol from Chen *et al.*[12] using the dialysis method. Generally, 10 mg of polymer was dissolved in 0.500 mL of acetone and shaken until completely dissolved. Then, DiI and DiO were added to the polymer solution so each was present in a 0.75% wt/wt (DiI or DiO/ polymer). Then, the solution was incubated for 30 minutes while protecting from light on an orbital shaker set at 200 RPM. After 30 minutes, each was added dropwise to 5 mL of rapidly stirring deionized water. This solution was stirred rapidly in the fume hood for 30 minutes followed by dialysis in 3.5 kDa molecular weight cut off (MWCO) dialysis membranes against 200 mL of deionized water for 48 hours at 4 °C. The dialysate was changed after 24 hours. The resulting FRET micelles were then removed from the dialysis units and stored in a 15 mL polypropylene centrifuge tube at 4 °C, wrapped with aluminum foil to protect from light until use.

3.9 Shear Force Experiments

The stock FRET micelles were removed from the refrigerator and let warm to room temperature. The sample to be tested was then diluted in a clean 15 mL polypropylene centrifuge tube with a micropipette and mixed by tilting the centrifuge tube gently to a 180° angle and back again several times. This gentle mixing was done for control samples, as well as samples to be vortexed. The sample was then vortexed for the

specified time using a vortexer at 3,000 RPM. Next, a 3 mL aliquot of the sample was

taken and placed into the 3 mL quartz cuvette with a transfer pipette just prior to

measurement. The pipetting was done slowly to decrease the amount of shear force

introduced. Instrument parameters for the fluorimeter used are described in **Chapter

3.2.2**.

4. RESULTS AND DISCUSSION

4.1 Synthesis of Macro-CTAs

4.1.1 Methyl Substituted Macro-CTAs. Macro-CTAs were synthesized using a previously reported protocol with modifications[23] by reacting commercially available poly(ethylene glycol) monomethyl ether (M_n = 2,000 g/mol, 4,000 g/mol, or 5,000 g/mol) with 2-bromopropionyl bromide for 24 hours in the presence of pyridine in DCM as solvent. Pyridine was used as a proton acceptor for the hydroxyl group proton on the mPEG following nucleophilic attack on the acyl bromide. The generated pyridinium bromide was removed by washing the reaction mixture with saturated ammonium chloride, saturated sodium bicarbonate, and then deionized water. The long mPEG chain is more soluble in DCM than in aqueous solution, especially in high salt concentrations were the ionic strength of the solution is high. The organic layer containing the crude product was then dried over magnesium sulfate before further purification by dropwise precipitation in cold diethyl ether. Pure product was obtained after collecting the precipitated product *via* vacuum filtration and drying under vacuum. A representative ^{1}H NMR spectrum for **1A** is shown below in **Figure 19** and **20**.

The methoxy group of the mPEG can be seen at 3.34 ppm, 3H singlet. The peaks from the CH$_2$ group of the PEG backbone adjacent to the ester linkage are also shifted (C in **Figures 19** and **20**) due to the electron withdrawing effect of the ester. The 1H, quartet α proton from the CH group (D in **Figures 19** and **20**) is attached to the strongly electron withdrawing carbonyl, and appears downfield ~4.36 ppm. The 3H doublet methyl group (E in **Figures 19** and **20**) on the β carbon is further away from any electron withdrawing

groups and is consequently more shielded and appears more upfield at 1.79 ppm. The

yields for **1A** and **3A** after purification was 80.1 % and 66.3 %, respectively. Compound

2A was used in the subsequent reaction as crude. The discrepancy in yield between **1A**

and **3A** is attributed to **3A** forming a white middle layer during the washing steps, which

was presumably monomethoxy poly (ethylene glycol) 5,000-2-bromoethyl ester.
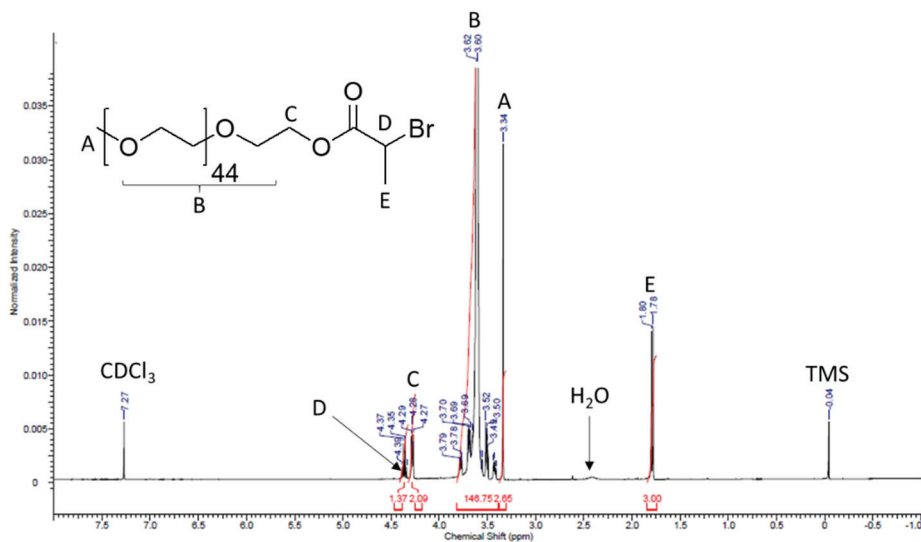
Figure 19. Full ^{1}H NMR spectrum of monomethoxy poly(ethylene glycol) 2,000-2-bromoethyl Ester (1A) in CDCl₃.
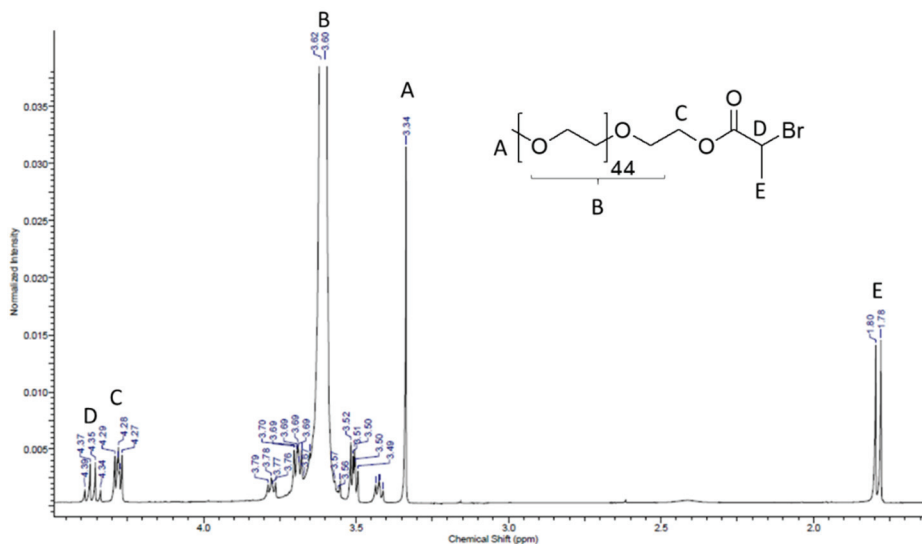
Figure 20. ^{1}H NMR spectrum of monomethoxy poly(ethylene glycol) 2,000-2-bromoethyl Ester (1A) in CDCl₃ from ~1 ppm to ~5 ppm.

After reacting the stock mPEG with 2-bromopropionyl bromide, the products **1A**, **2A**, and **3A** were reacted with excess potassium *O*-ethyl xanthate in the presence of pyridine in DCM at room temperature for 24 hours. Pyridine was used as an activator, as the potassium *O*-ethyl xanthate is a poor nucleophile. After reacting for 24 hours, the reaction mixture was again washed with saturated ammonium chloride, saturated sodium bicarbonate, and a small amount of deionized water to remove any potassium bromide formed during the reaction, or any unreacted potassium *O*-ethyl xanthate. The organic layer was dried over anhydrous magnesium sulfate and precipitated dropwise into cold diethyl ether. The precipitate was collected via vacuum filtration through a Gooch funnel and excess solvents were removed via vacuum to yield compounds **1B**, **2B**, and **3B**. A representative ^{1}H NMR is shown below in **Figure 21** for **2B**.
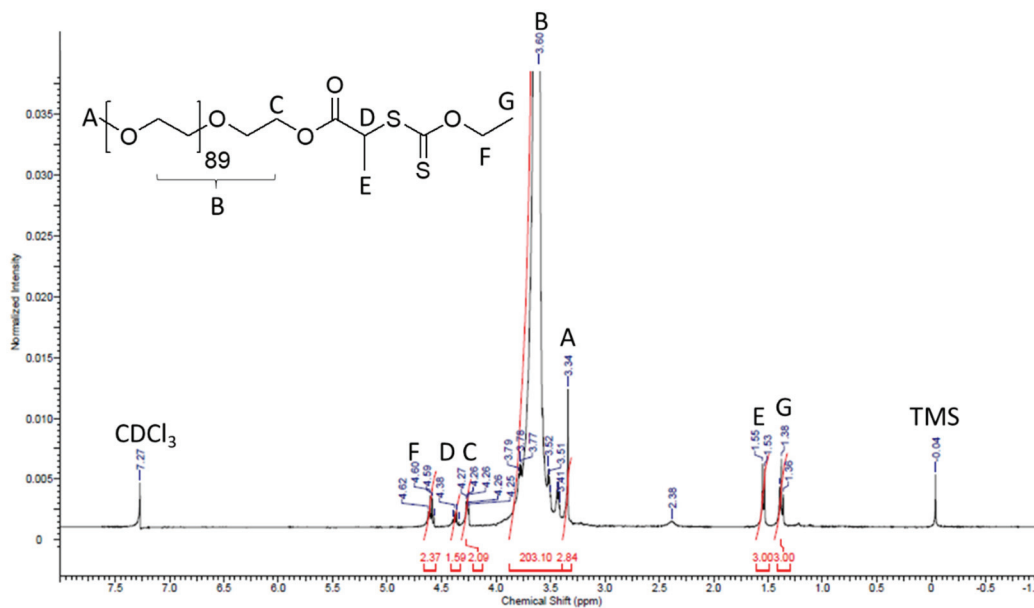
Figure 21. Full ^{1}H NMR spectrum of *S*-2-(monomethoxy poly(ethylene glycol) 4,000 propionate)-(*O*-ethyl xanthate) (**2B**) in CDCl₃.

The ^{1}H NMR in **Figures 21** and **22** is consistent with literature.[20] The appearance of the xanthate peaks are seen in the spectrum. The CH₂ group from the xanthate (labeled

F in **Figures 21** and **22**) is fairly deshielded from the electron withdrawing oxygen adjacent and the thioester in close proximity. Consequently, this peak is seen at 4.60 ppm as a 2H quartet. The CH₃ group of the xanthate is relatively shielded because of the distance from electron withdrawing groups. Consequently, this peak is seen downfield at 1.38 ppm as a 3H triplet.
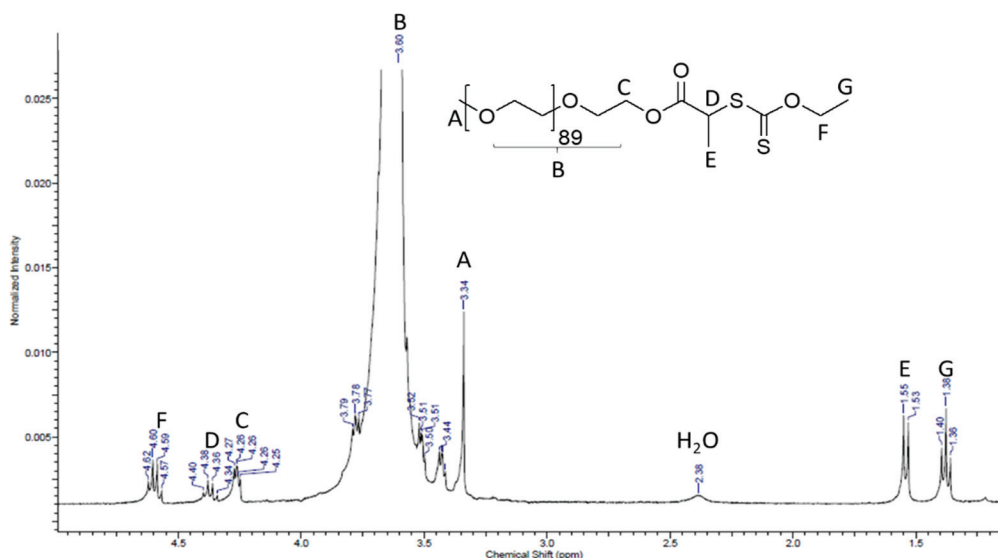
Figure 22. Important peaks of ^{1}H NMR spectrum of S-2-(monomethoxy poly(ethylene glycol) 4,000 propionate)-(O-ethyl xanthate) (**2B**) in CDCl₃.

4.1.2 Unsubstituted Macro-CTAs. The methylene peak (D in the **Figure 23**) is not well resolved from the PEG backbone, and was therefore not integrated as any integration of this peak would be inaccurate. The methylene peak, however, is a singlet as would be expected. The CH₂ group of the PEG backbone adjacent to the newly formed ester linkage is shifted further downfield than the other PEG backbone protons (peak C) as is expected due to the electron withdrawing effect of this ester linkage. As is usual for this CH₂ group, it is not cleanly split and appears as a 2H multiplet. The methoxy group

appears at 3.36 ppm as a 3H singlet.
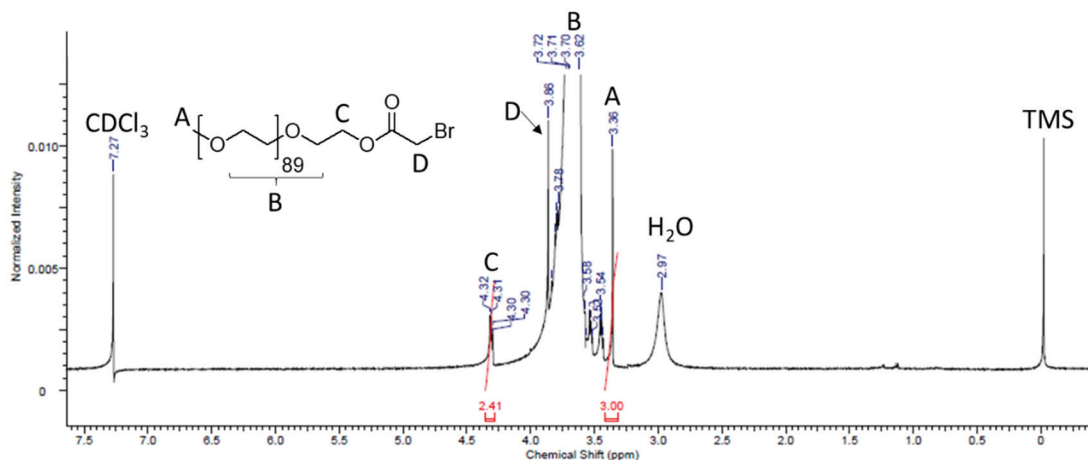
Figure 23. ^{1}H NMR of monomethoxy poly(ethylene glycol) 4,000-bromomethyl ester (**4A**) in CDCl$_3$.

^{1}H NMRs in **Figures 24** and **25** indicating the formation of product **4B**. Importantly, the methylene group from protons D are shifted further downfield than the intermediate product, **4A** due to the stronger electron withdrawing effect of the xanthate. D appears as a 2H singlet as expected and is now resolved well enough from the PEG backbone (protons B) for accurate integration. Peaks E and F are also present in the spectrum as a 2H quartet and 3H triplet, respectively. E appears downfield at 4.60 ppm due to the strong electron withdrawing effect of the adjacent oxygen and xanthate. On the contrary, F appears upfield caused by more shielded protons due to the distance from any electron withdrawing groups. Structures of all macro-CTAs are shown in **Figure 26**.
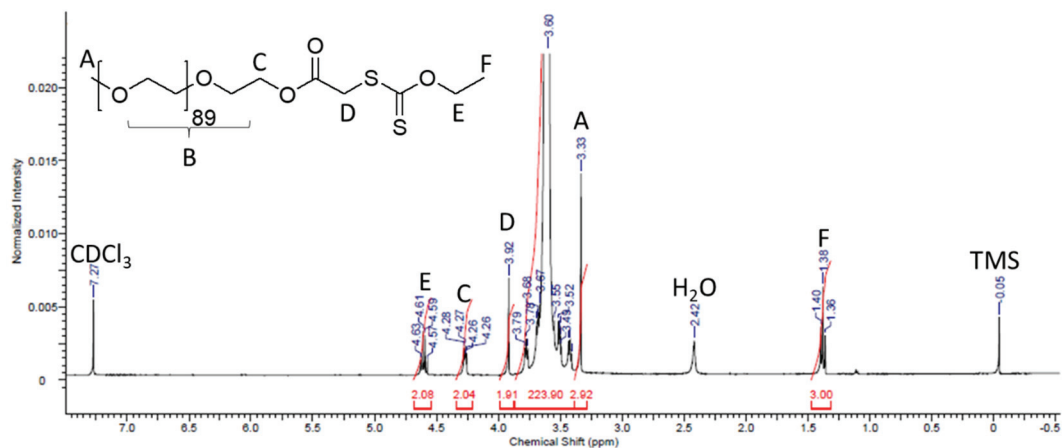
Figure 24. ^{1}H NMR of S-(monomethoxy poly(ethylene glycol) 4,000 acetate)-(O-ethyl xanthate) (4B) in CDCl$_3$.
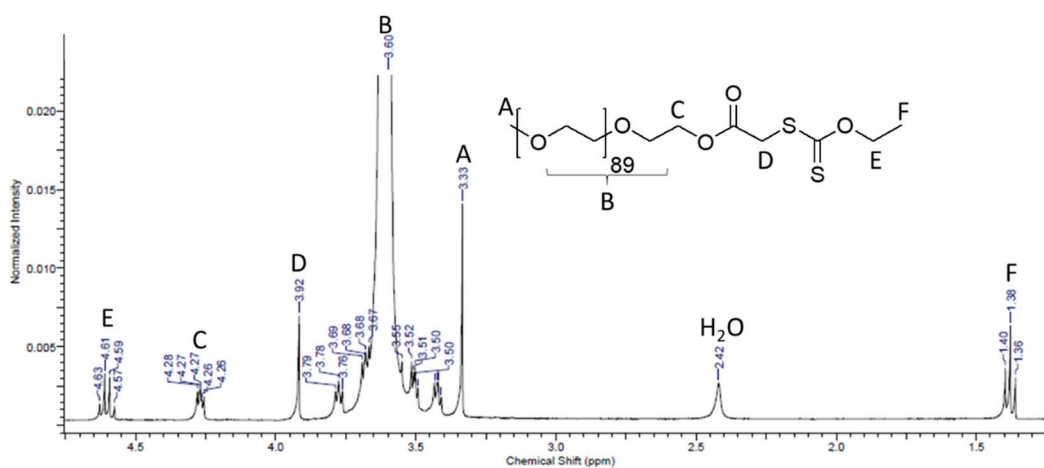
Figure 25. ^{1}H NMR of S-(monomethoxy poly (ethylene glycol) 4,000 acetate)-(O-ethyl xanthate) (4B) in CDCl$_3$ showing only important peaks.

n = 45 (1B), n = 90 (2B), n = 112 (3B),
or

n = 90 (4B)
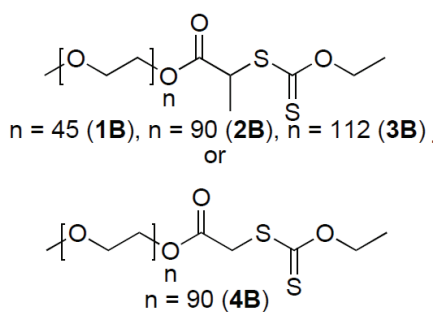
Figure 26. Structures of synthesized macro-CTAs.

34

4.2 RAFT Polymerization

A typical RAFT polymerization involved removal of the inhibitor from both THF (stabilized with BHT) and VAc (stabilized with HQ) by passing each through a short column of basic alumina before use and combining AIBN (the initiator), the macro-CTA, VAc, and THF (as solvent) in a 15 mL pear-shaped flask equipped with a spin vane. Four freeze-pump-thaw cycles were then performed to remove all oxygen from the reaction vessel and any dissolved in the reaction media. The vessel was then filled with nitrogen gas and attached to a water condenser unless otherwise noted. The reactions were performed under a steady flow of nitrogen gas and a silicone oil bath was used to uniformly heat the reaction. The resulting products were an opaque solid after purification.

4.3 RAFT Polymerization of Vinyl Acetate with 2B

Since it is of intermediate length, **2B** was first used for RAFT Polymerization (**Figure 27**). A representative ^{1}H NMR for Rxn 5 is shown below in **Figure 28**.
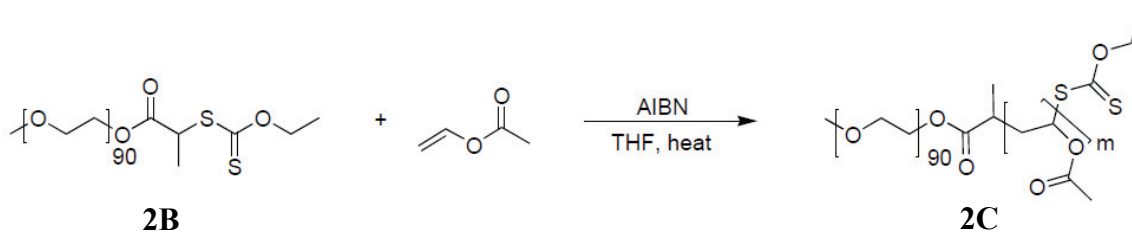
Figure 27. RAFT polymerization of vinyl acetate with macro-CTA **2B** to yield block copolymer **2C**.
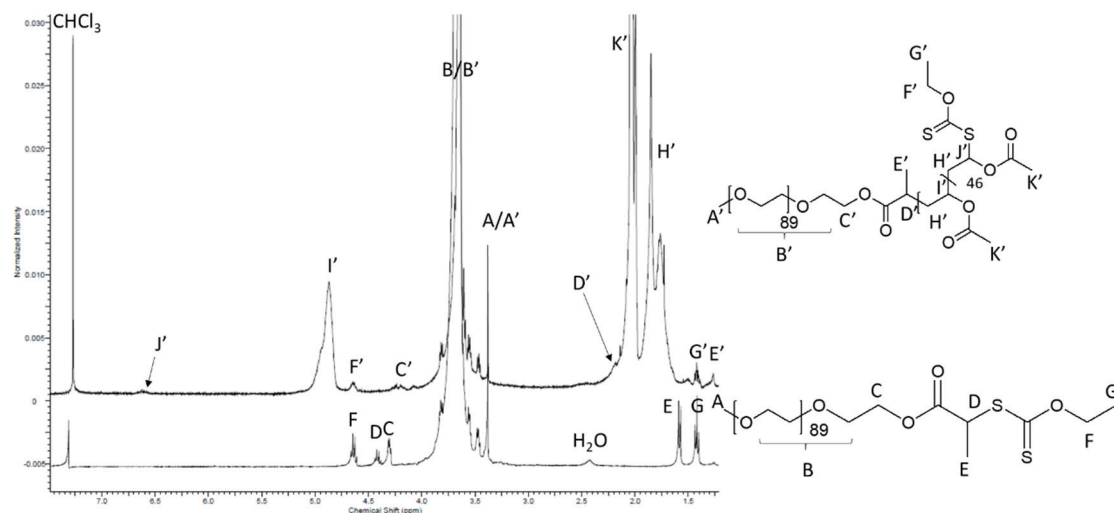
Figure 28. Stacked ^{1}H NMR of **2B** (bottom line) and mPEG (4000)-*b*-PVAc47 (top line; product of Rxn 5 in **Table 1**).

^{1}H NMR shows the emergence of peak J, and the shifting of peak D to D', reflecting the more shielded proton found in the block copolymer, and E to E' for similar reasons, though a smaller shift downfield is seen. The broad peaks are a reflection of the tacicity created upon polymerization and is consistent with literature[20]. Degree of polymerizations were calculated by setting the integration of the PEG backbone plus methoxy group (A' and B' in **Figure 28**) to 361 for mPEG90 for a reference integration. The integration values of K' and H' were then added together and divided by 5 (the number of protons) to obtain the degree of polymerization. In most cases, this value agreed very well with the value obtained by integrating peak I alone.

4.4 Optimization of Reaction Conditions with macro-CTA 2B with Vinyl Acetate

Table 1 shows the RAFT Polymerization trials with **2B**. The initial goal was to synthesize an mPEG (4000)-*b*-PVAc block copolymer with the same number of vinyl acetate repeat units as repeat units of PEG in mPEG (4000), or 90. The first reaction (Rxn

1) was performed similar to litearture[20], but the solvent ratio (mL of THF/mol of macro-CTA) was increased from 13.7 to 80.9 to solubilize the macro-CTA at room temperature. At a solvent to macro-CTA ratio of ~13.7, very little of the macro-CTA was soluble at room temperature. However, even at a reaction time of 48 hours, only 4 repeat units of VAc were incorporated into the product at 60 °C. The same reaction was then repeated for Rxn 2, but the temperature was increased to 80 °C. Because this is higher than the boiling point of VAc and THF, this reaction was carried out in a pressure flask. This reaction also had a very low degree of polymerization after 15 hours, only 10 VAc units. This suggested that temperature was not the major cause of the problem. In Rxn 3, the monomer: macro-CTA molar ratio was increased from 97.2 to 195.0, more than double and the solvent ratio was decreased to 40.6. For a reaction time of 21 hours 20 minutes at 66 °C, 31 VAc units were calculated *via* ^{1}H NMR , indicating that the monomer: macro-CTA ratio and solvent ratio are vital in yielding high degrees of polymerizations. This, however, is still far from the 88 VAc units literature reports.[20] For Rxn 4, approximate ratios from literature were used, and after 17 hours 47 minutes, 20 VAc units were added. Rxn 5 doubled the monomer concentration from Rxn 4 and after 24 hours yielded only 47 VAc units were calculated *via* ^{1}H NMR. This is in contrary to literature, with a similar macro-CTA with 75 PEG repeat units.[20]

Table 1. RAFT polymerizations of vinyl acetate with *S*-2-(monomethoxy poly(ethylene glycol) 4,000 propionate)-(*O*-ethyl xanthate) (macro-CTA **2B**).

Rxn	Solvent	macro-CTA[A] : AIBN : VAc : solvent[B]	Temperature (°C)	Reaction time	Degree of Polymerization[C]
1	THF	1 : 0.253 : 97.2 : 80.9	60	48 hrs	4.02
2	THF	1 : 0.253 : 97.2 : 80.9	80	15 hrs	10.25
3	THF	1 : 0.253 : 195 : 40.6	66	21.3 hrs	30.55
4	THF	1: 0.254 : 96.5 : 11.7	56	17.8 hrs	20.17
5	THF	1 : 0.254 : 194 : 11.7	57	24 hrs	47.44

A: CTA: Chain transfer agent. **B**: macro-CTA: AIBN: VAc: Solvent expressed as molar ratios to **2B**, except solvent which is expressed as milliliters of solvent per mmol of macro-CTA. **C**: Degree of polymerizations are calculated from integration values on each ^{1}H NMR, and represent the repeat units of vinyl acetate in each synthesized block copolymer.

4.5 RAFT Polymerization of Vinyl Acetate with 1B

After these series of reactions, we hypothesize that the long mPEG chain retarded the polymerization, sterically blocking the addition of additional monomers to the macro-CTA. RAFT polymerization of VAc with **1B** (*S*-2-(monomethoxy poly(ethylene glycol) 2,000 propionate)-(*O*-ethyl xanthate)) (**Figure 29**), which differs from **2B** only by PEG chain length (45 repeat units and 90 repeat units, respectively), in THF at 58 °C was then tested. The macro-CTA : AIBN : monomer : solvent ratio for this reaction were: 1 : 0.252 : 197 : 11.9 , similar to Rxn 5. The degree of polymerization for this was 153, indicating that the PEG length does, in fact, play an important role of the polymerization kinetics. It is important to note that reference 20 uses mPEG with an average molecular mass of 3,300 g/mol, between that of **1B** and **2B**.
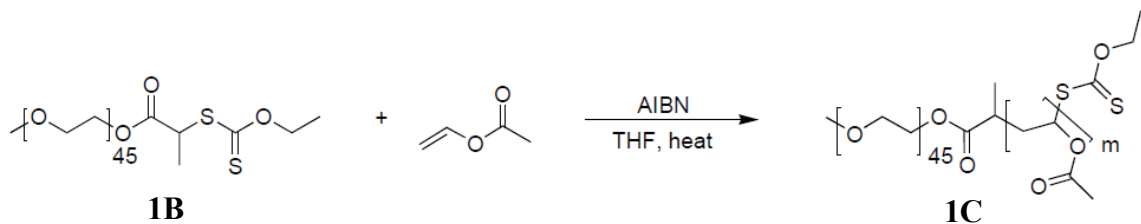
Figure 29. RAFT polymerization of vinyl acetate with macro-CTA **1B** to yield block copolymer **1C**.

4.6 RAFT Polymerization of Vinyl Acetate with 4B

In order to study the effect of methyl substitution on the R group, another macro-CTA was synthesized for mPEG (4000), **4B**. The macro-CTA : AIBN : Monomer : solvent ratio for this reaction were: 1: 0.259 : 196 : 11.4 at 58 °C for 24 hours, very similar to the RAFT polymerization of **1B** with VAc (**Figure 30**). The degree of polymerization was found to be 120. It is still unknown at this point what causes the significantly different polymerization rate between **2B** and **4B**, given that the difference between the two macro-CTAs is the R group. Generally, the Z group is reported to have more influence on polymerization kinetics since it can either stabilize the intermediate radical (3 and 4 in **Figure 8**), or destabilize the intermediate and this is well reported.[18-20,26,28,29] However, it is also known that the R group influences reactivity. Importantly, the R group influences radical addition to the macro-CTA since it influences the C=S reactivity, influences the rate of fragmentation from the intermediate and therefore must be a good homolytic leaving group. Hence, this effects the rate of propagation since the R group must rapidly reinitiate propagation.[29] In this instance, however, we believe that it is the increased reactivity of the radical R group following homolytic cleavage in the pre-equilibrium step and reinitiation. The resulting radical R groups for **2B** and **4B** are shown

in **Figure 31**.
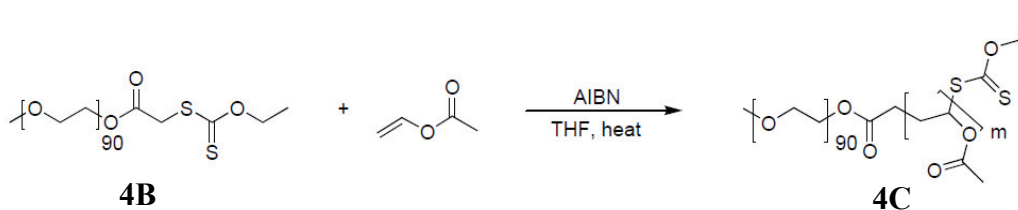
Figure 30. RAFT polymerization of macro-CTA **4B** with vinyl acetate to yield block copolymer **4C**.

We speculate that this is the rate limiting step in the polymerization for this macro-CTA, but more experimentation is necessary to determine this conclusively. It is important to note here that the difference in the electron density on the α-carbon on the intermediates shown in **Figure 31**. More electron density will be present on α-carbon for the radical generated from **2B** due to the methyl substitution group, leading to greater stability and, as a consequence, lower reactivity.

Structures of all block copolymers can be found in **Figure 32**. The optimized RAFT polymerization reactions are summarized in **Table 2**. Because of the similarity in hydrophobic block length, the resulting block copolymer from Rxn 5, which utilized macro-CTA **2B**, was used in subsequent characterization.

4B

2B
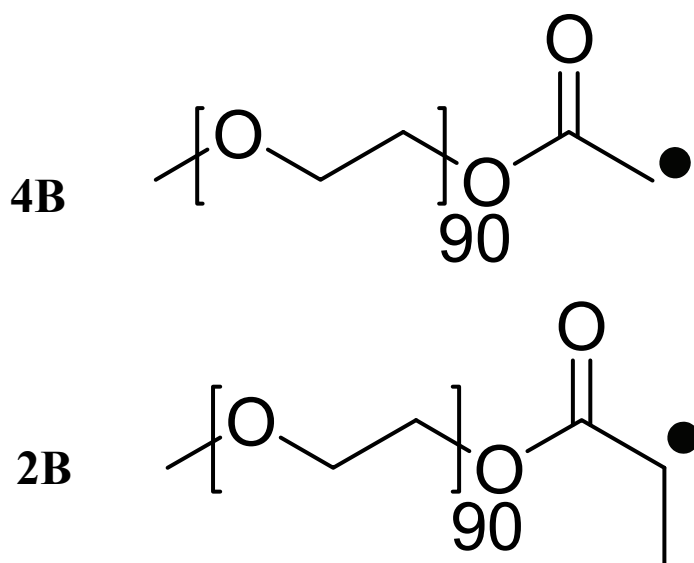
Figure 31. Resulting radicals from homolytic cleavage of **4B** (top) and **2B** (bottom).

n = 45 (**1C**), 90 (**2C**), 112 (**3C**)   n = 90 (**4C**)
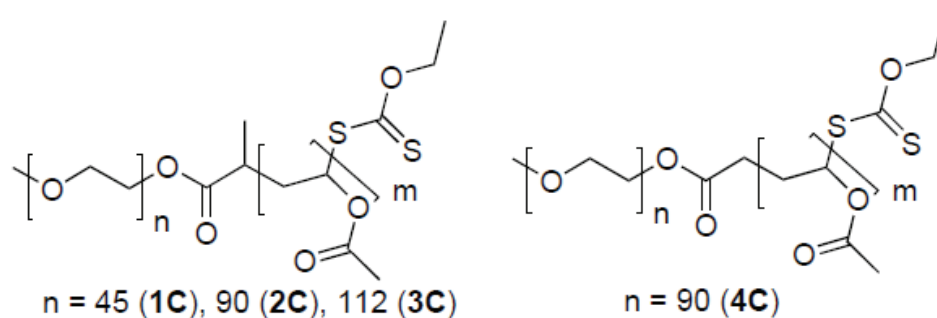
Figure 32. Structures of block copolymers.

Table 2. Optimized RAFT polymerization conditions.

Rxn[A,B]	Macro-CTA	Temperature (°C)	Reaction Time	Degree of Polymerization[C]
5	**2B**	57	24	47
6	**1B**	58	24	153
7	**4B**	58	24	120

A: All reaction conditions are similar to that from Rxn 5 in **Table 1**: macro-CTA: AIBN: VAc: THF: 1 : 0.254 : 194 : 11.7. **B:** macro-CTA: AIBN: VAc: Solvent expressed as molar ratios to the respective macro-CTA, except solvent which is expressed as milliliters of solvent per mmol of macro-CTA. **C:** Degree of polymerizations are calculated from integration values on each ^{1}H NMR, and represent the repeat units of vinyl acetate in each synthesized block copolymer. The Degree of Polymerizations are rounded to the nearest whole number.

4.7 Proof of Concept with PEG5000-*b*-PLA5000

To establish the proof-of-concept, we used a commercially available amphiphilic block copolymer poly(ethylene glycol) 5000-*b*-poly(lactic acid) 5000 (PEG5000-*b*-PLA5000)) (**Figure 33**). Micelles with encapsulated DiI/DiO (0.75 % wt/wt DiI or DiO/polymer) were prepared by the dialysis method, as previously reported.[12,13] These micelles with the encapsulated FRET pair (DiI/DiO) are referred to as PEG-PLA FRET micelles hereafter.
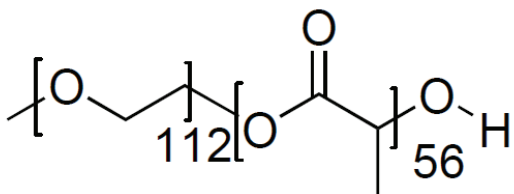
Figure 33. Structure of PEG(5000)-*b*-PLA(5000).

The resulting stock solution of our PEG-PLA FRET micelles was approximately 1.9 mg/mL. At first the stability of these micelles were investigated. The stock PEG-PLA FRET micelles were diluted 1/100 with deionized water. After gentle inversion to mix, the fluorescence was measured at 30 seconds, 5 minutes, 10 minutes, 20 minutes, and 30 minutes to establish the stability of the PEG-PLA FRET micelles after dilution. The samples were excited at 425 nm and the emission spectrum from 450 nm – 650 nm was recorded. As expected, a rather large acceptor peak (DiI) ~ 570 nm and a small donor peak ~505 nm (DiO), showing that both fluorophores were present in the core of the micelle. Furthermore, virtually no intensity loss of the acceptor peak is seen over the lifetime of the experiment (30 minutes), confirming the stability of the PEG-PLA FRET micelles diluted 1/100 in deionized water (**Figure 34**).
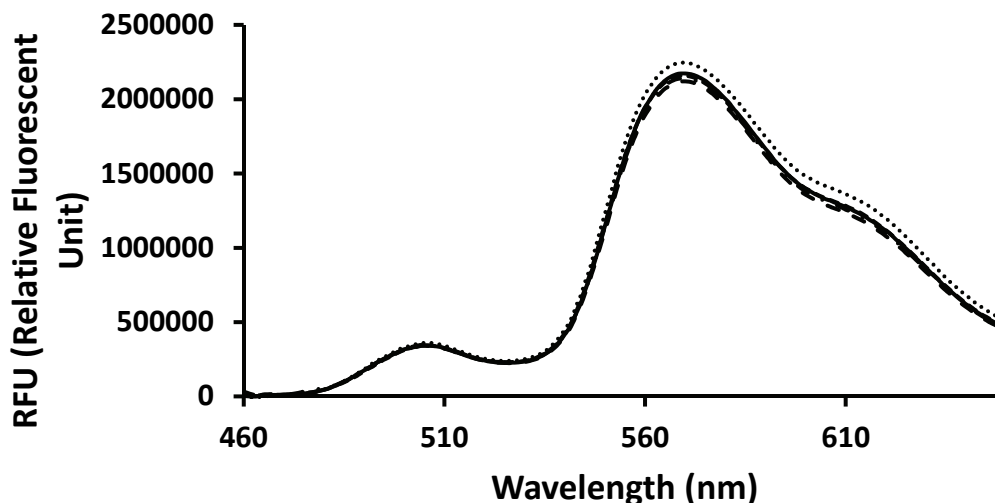
Figure 34. PEG-PLA FRET micelle stability diluted 1/100 and deionized water at 30 seconds, 5 minutes, 10 minutes, 20 minutes, and 30 minutes.
·········· After 30 seconds, ———— After 5 minutes, – – – After 10 minutes, – · – · After 20 minutes, and – – – – – After 30 minutes.

The PEG-PLA FRET micelles were diluted 1/100 in 50 % (v/v) and 100 % acetone. Both the polymer and the FRET pair are anticipated to be soluble in acetone. **Figure 35** shows the resulting fluorescence spectra of these samples.

As previously shown, 1/100 diluted PEG-PLA FRET micelles in water (dashed line in **Figure 35**) shows a large acceptor peak, with a small donor peak when excited at 425 nm. In contrast, when the concentration of acetone is increased to 50%, the donor peak gains intensity and the acceptor peak loses intensity. We are attributing this to the partial release of the FRET pair from the micelles and into the bulk solution; in this case, a portion of the donor and acceptor would no longer be in close proximity, and FRET would not occur. When the acetone concentration was increased to 100 %, the acceptor peak is diminished and the donor peak dominates the spectrum. This is indicative of total release of the FRET pair from the micelles.

43
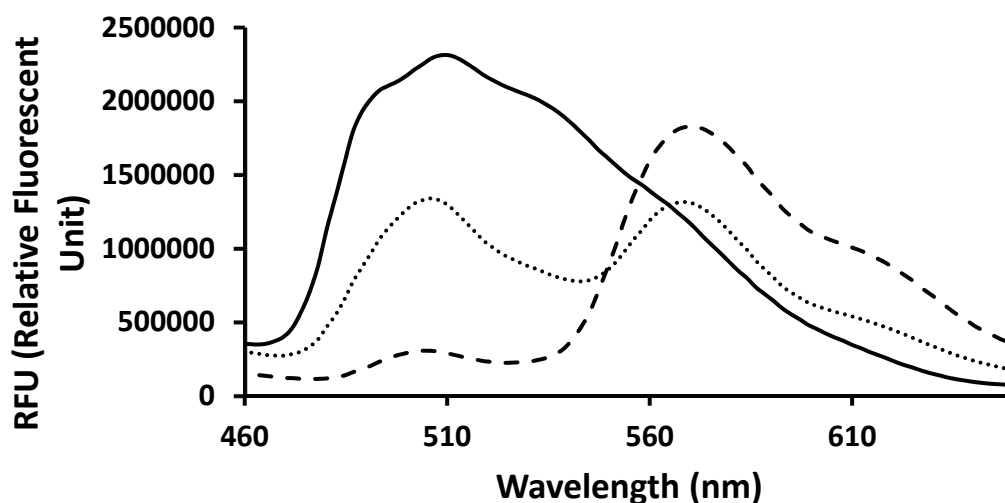
Figure 35. Fluorescence Spectra of PEG-PLA FRET micelles diluted 1/100 in deionized water, 50 % (v/v) acetone/water, and 100 % acetone.
- - - - 1/100 in deionized water, ········· 1/100 in 50% (v/v) acetone/water, and ——— 1/100 in 100 % acetone.

4.8 Force-responsiveness of PEG-PLA FRET Micelles

Next the PEG-PLA FRET micelles were subjected to shear forces *via* vortexing the diluted samples for 30 seconds at 3,000 rpm immediately before fluorescence measurements. This speed was chosen to ensure the maximum amount of shear force was introduced. First, a fluorescence spectrum of 1/100 diluted PEG-PLA FRET micelles in water was taken and then this sample was subjected to 30 seconds under vortex, measured, and then an additional 60 seconds under vortex. A photobleach test was also carried out to establish that any decrease in fluorescence intensity was not due to photobleaching while in the fluorimeter excitation beam. The results are shown in **Figure 36.** Very modest decreases in both the donor fluorescence intensity and acceptor fluorescence intensity are seen after each vortex. We attribute the decrease in both to release of the FRET pair from the PEG-PLA micelles. Interestingly, however the donor

intensity also drops. We attribute this to the precipitation/aggregation of the fluorophores due to the very poor solubility in aqueous solution upon release from the micelles. It is important to note that this fluorescence was not recovered over time.
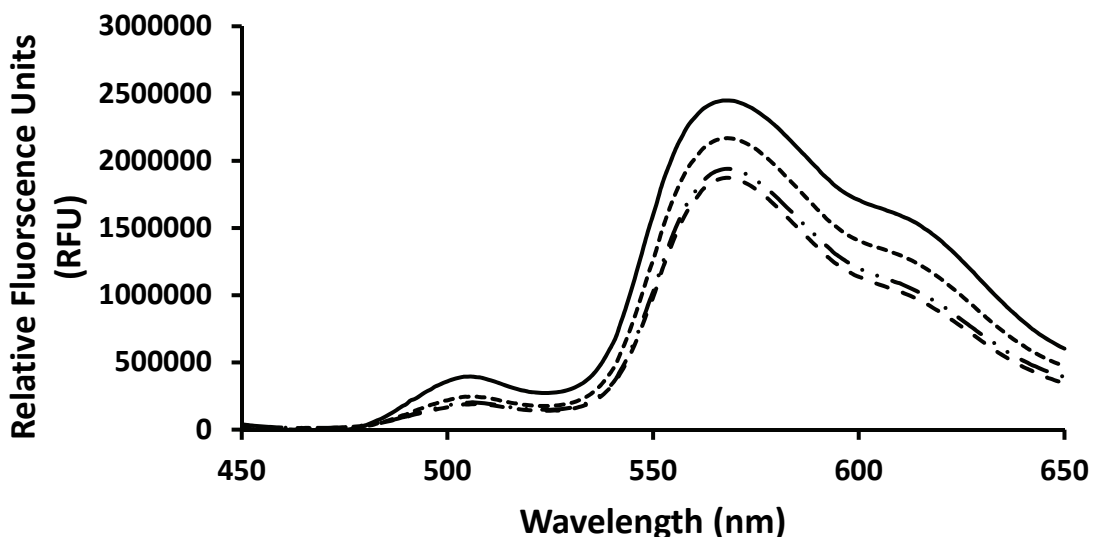
Figure 36. Fluorescence Spectra of 1/100 Diluted PEG-PLA FRET Micelles in water before and after vortex. ———— 1/100 in water, ━ ━ ━ ━ ━ 1/100 in water after 30 second vortex, ━━ ˙ ˙ 1/100 in water after 60 second vortex, ━ ━ ━ photobleach control: 1/100 in water after 60 second vortex + 10 minutes excitation in fluorimeter.

Since only a very modest decrease in acceptor intensity was seen after subjecting the PEG-PLA FRET micelles to vortex (shear force), a similar experiment was carried out, with the inclusion of 10 % acetone in the final 1/100 dilution to provide a basis of comparison for the results with the PEG-PVAc micelles. The result is shown in **Figure 37** for a 1/100 dilution of PEG-PLA FRET micelles in 10 % acetone (v/v). As shown in

the spectra, the acceptor intensity drops significantly after vortexing, which is indicative

of release of the FRET pair from the micelles.
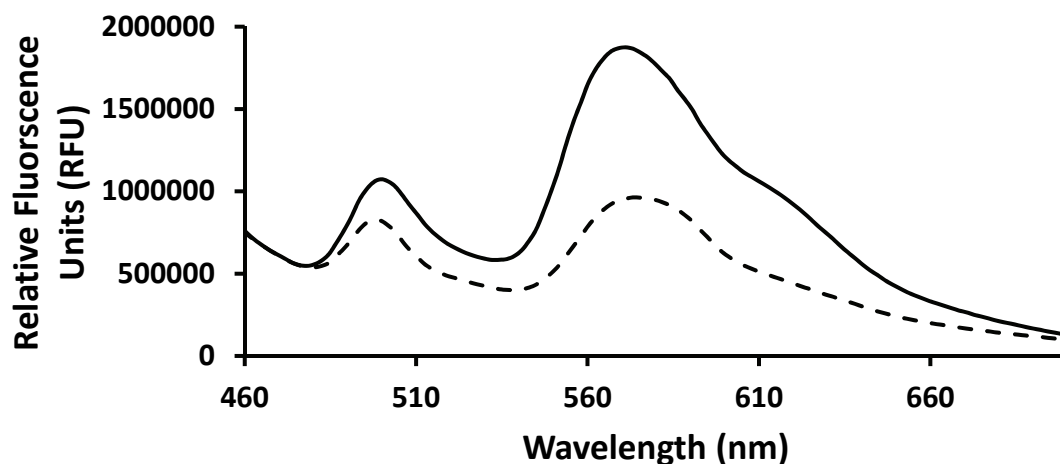
Figure 37. Fluorescence Spectra of 1/100 Diluted PEG-PLA FRET micelles in 10 %
acetone (v/v) before and after vortexing. Solid line: before vortexing. Dashed line: after
30 second vortex.

4.9 Conclusion from PEG-PLA FRET Micelles

The intensity of the acceptor peak was higher in water than acetone, indicating the

DiO and DiI were encapsulated within the PEG-PLA FRET micelles. The data also

suggests that PEG-PLA FRET micelles can be broken by the introduction of shear force

in the presence of acetone, releasing the encapsulated hydrophobic material. Since a

decrease in intensity in both the donor and acceptor peak was observed, we attribute this

to the precipitation of DiO and DiI from solution after being released.

4.10 mPEG-*b*-PVAc FRET Micelles

FRET micelles were created with block copolymer **2C** (from Rxn 5), which

yielded 47 vinyl acetate units in the hydrophobic portion, as determined by ^{1}H NMR.

FRET micelles were prepared as described in the EXPERIMENTAL section using the

dialysis method with 0.75 % (wt/wt) DiO/DiI as the encapsulated hydrophobic FRET

pair. As with the model system, PEG(5000)-b-PLA(5000), it was first necessary to

confirm that the DiO and DiI are encapsulated in the micelle and not dispersed in the bulk

solution. To confirm this, a fluorescence spectrum of these FRET micelles (mPEG$_{90}$-b-

PVAc$_{47}$) in both water and acetone following a 1/100 dilution (**Figure 38**) was measured.
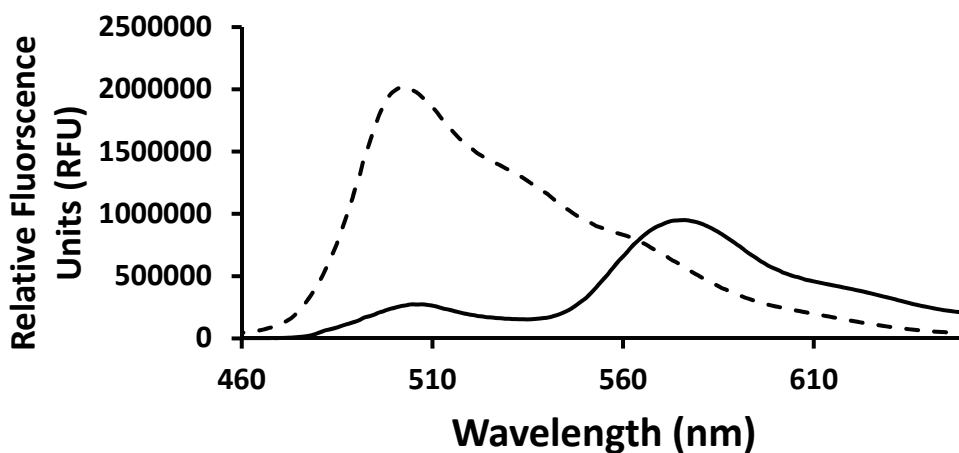
Figure 38. Fluorescence spectrum of mPEG$_{90}$-b-PVAc$_{23}$ FRET micelles in acetone.
Dashed line: 1/100 diluted in acetone. Solid line: 1/100 diluted in water.

In water, a larger peak for the acceptor is seen ~570 nm when only the donor is

excited (at 425 nm) (solid line). This is indicative of an encapsulated FRET pair since

FRET is highly distance dependent. Conversely, when diluted 1/100 in acetone, virtually

no acceptor peak is seen and the donor peak dominates the fluorescence spectrum,

indicating the FRET pair are free in solution. This experiment confirms micelle

encapsulation of the FRET pair.

4.11 Measuring Force-responsiveness of mPEG$_{90}$-*b*-PVAc$_{47}$ FRET Micelles

A control experiment was then performed to confirm that the fluorescence intensity loss was not due to degradation of the micelles over time, possibly from being diluted lower than the critical micelle concentration (CMC). To measure this, the stock sample of mPEG$_{90}$-*b*-PVAc$_{47}$ FRET micelles were diluted 1/100 (v/v) in deionized water and a fluorescence spectrum was taken after 2 hours at room temperature. The resulting spectrum is shown in **Figure 39**. A slight decrease is seen in the fluorescence intensity of the acceptor peak, but a rather large decrease is seen in the donor intensity, indicating some micelle breakage after 2 hours. In order to minimize degradation of the micelles before subjection to shear forces, we plan to test the polymer with longer hydrophobic chain length which should lower the CMC.

The second step was to confirm that these micelles are able to be broken under a reasonable amount of force. To test this, mPEG$_{90}$-*b*-PVAc$_{47}$ FRET micelles were diluted 1/100 (v/v) in deionized water and subjected to vortex at 3,000 rpm and the fluorescence spectrum measured. **Figure 39** shows a drop in acceptor and donor intensity upon 30 seconds of vortexing. The fluorescence intensity loss of both acceptor and donor peaks indicates release of the FRET pair from the core of the micelles followed by precipitation/aggregation. A duplicate sample was also prepared and subjected to vortex at 3,000 RPM for 2 minutes, and a further decrease in fluorescence intensity of both acceptor and donor were seen, a larger decrease than that of 30 second vortex. This indicates that not all micelles were broken upon exposure to this shear force for 30 sec.
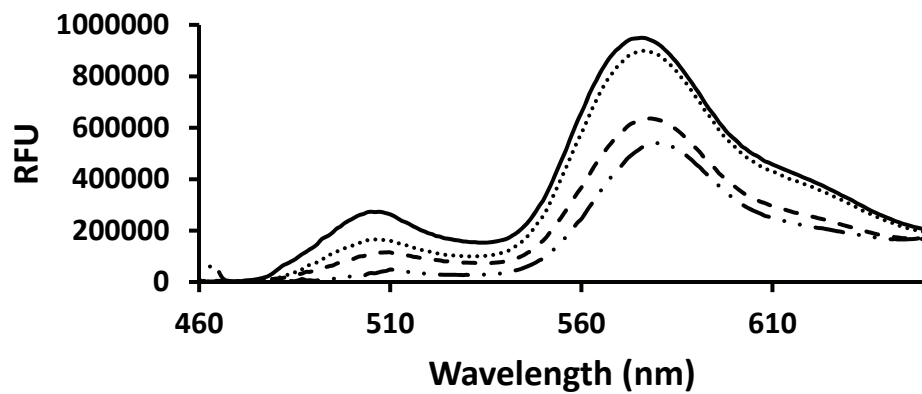
Figure 39. Fluorescence spectra of mPEG$_{90}$-*b*-PVAc$_{23}$ FRET micelles after vortex. ———— 1/100 diluted in DI H$_2$O; ‒ ‒ ‒ 1/100 diluted in DI H$_2$O after 30 second vortex; —·· 1/100 diluted in DI H$_2$O after 2 minute vortex; ·········· 1/100 diluted in DI H$_2$O after 2 hours. Excitation: 425 nm.

5. CONCLUSION

The successful synthesis of four macro-CTAs with $mPEG_{45}$, $mPEG_{90}$, and $mPEG_{112}$ has been described. During the RAFT Polymerization trials, it was found that both chain length and R group play a large role in the polymerization kinetics; under the same polymerization conditions, the methyl substituted $mPEG_{90}$ macro-CTA (**2B**) yielded the polymerization up to 47 VAc repeat units, whereas the methyl substituted $mPEG_{45}$ macro-CTA (**1B**) and unsubstituted $mPEG_{90}$ macro-CTA (**4B**) yielded the polymerization up to 153 and 120 VAc repeat units, respectively. After synthesizing these amphiphilic diblock copolymers, shear force-responsiveness of block copolymer micelles was assessed utilizing DiO and DiI as fluorescent reporters for micelle stability. Preliminary results suggest the shear force-responsiveness of these amphiphilic diblock copolymers may be tuned by modifying the chemical structures of block copolymers although more experiments are necessary to confirm the validity of our approach. Future studies for micelle characterizations will include rheometery as a means of quantifying the amount of applied shear force.

6. INTRODUCTION

In this work, we set out to synthesize sugar-fluorophore conjugates by direct conjugation of sugar-azide and fluorophores with terminal alkynes by utilizing copper (I)-catalyzed alkyne-azide cycloaddition (CuAAC) **(Figure 40)**.[30] Three inexpensive fluorophores are used: rhodamine B, fluorescein, and 6-hydroxycoumarin, each fluorescing a different color. Since the fluorophores are covalently linked to the carbohydrate, no reaction with the bacteria is necessary. Once these sugar-fluorophore conjugates are synthesized, screening will take place as shown in **Figure 41**. Incubation of bacteria with the sugar-fluorophore conjugates and subsequent washes, followed by fluorescence measurements will allow for determination of the fluorescent ratios which indicate the rate of surface binding and internalization of the fluorescent probes. The long term-goal is to utilize this ratio for bacterial identification, similar to Otten *et al.*[31] The advantage of this system is the utilization of fluorescence ratiometric detection, and fast screening.
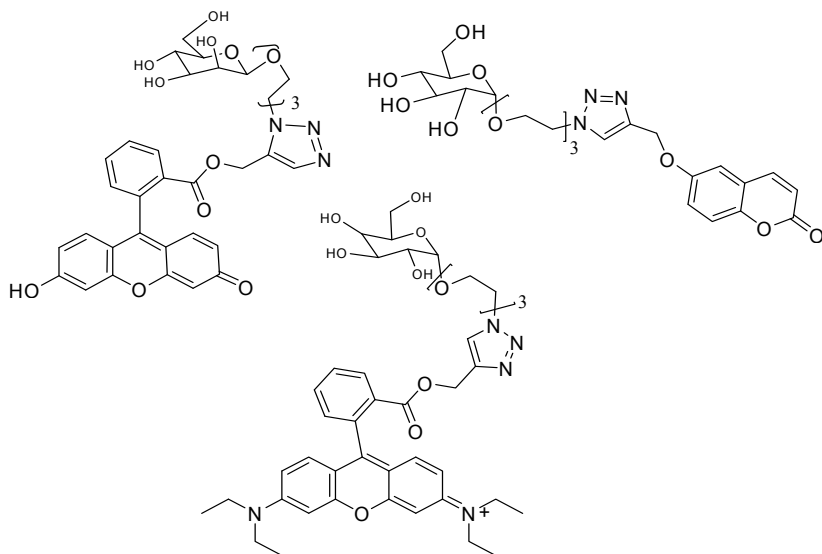
Figure 40. Structures of sugar-fluorophore conjugates to be synthesized.
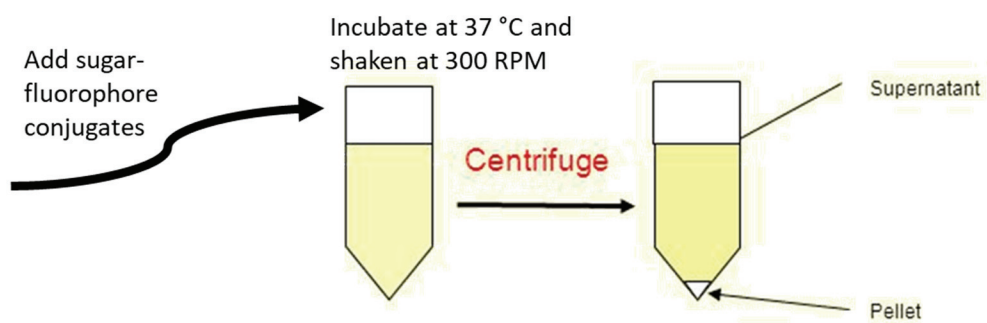

Figure 41. Schematic depiction of sugar-fluorophore screening.

7. LITERATURE REVIEW

7.1 Carbohydrate-based Arrays

Recently, carbohydrate-based arrays have been used to discriminate between both mammalian cells and bacterial cells due to the inexpensive nature and rapid detection.[31,32,33] In particular, bacterial detection is of significant interest as most current clinical detection methods approved by the FDA rely on tedious culturing steps.[34] This is further complicated as it has been estimated that only ~1 % of bacteria are culturable on standard culture media.[35-37] PCR-based detection processes have quickly gained popularity as an alternative. Two popular PCR based processes are: analysis of the full genome of bacterial species through comparison with a database[38,39], or Ibis, which involves selective PCR of a specific element of DNA. Though PCR methods can be very fast (Ibis takes only ~6 hours), both are expensive. Ibis, for example, relies on the use of a mass spectrometer, an instrument not accessible in most clinical settings. Both also rely on the extraction of nucleic acids from within the bacteria, causing another problem: Gram-positive bacteria can be very difficult to lyse due to their thick peptidoglycan wall.[37]

Generally, a carbohydrate-based microarray relies on the binding, or internalization of (usually) fluorescently labeled carbohydrates and subsequent imaging. Some carbohydrates bind to the bacterial surface because the carbohydrates are lectins, which specifically bind to proteins on the cell surface, while others are internalized through specific sugar transporters, such as the maltodextrin transporter in *E. coli*.[31,40,41] Transporters are generally specific for a carbohydrate, or a small number of carbohydrates and are genetically regulated. Chen *et al.*[41] showed this discrimination

between glucose, galactose, and sucrose (**Figure 42**), while Ning *et al.*[40] utilized the

maltodextrin transporter in *E. coli* to detect *E. coli* with high specificity in mice *in vivo*
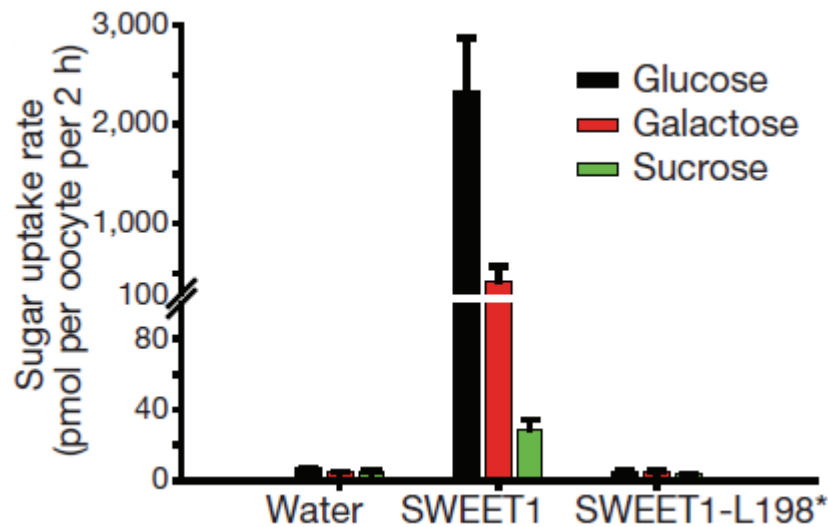
(**Figure 43**).[45]

Figure 42. Sugar internalization between of glucose, galactose, and sucrose in two different bacteria. Reproduced from reference 40 with permission. 2010 Copyright Springer Nature.
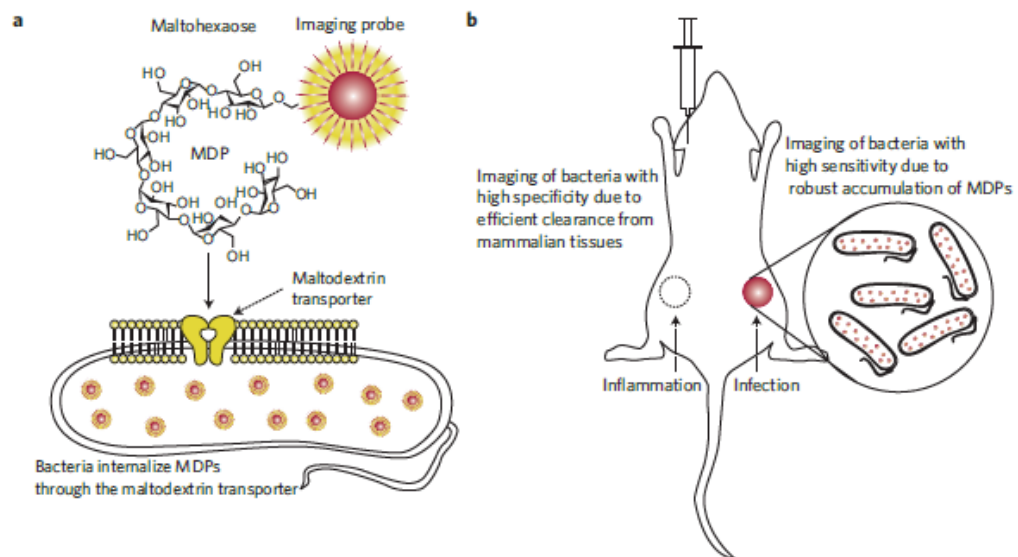

Figure 43. Detection of *E.coli in vivo* in mice utilizing the maltodextrin transporter. Reproduced with permission from reference 45. 2011 Copyright Springer Nature.

While some carbohydrates are highly specific, other may be more promiscuous in their binding, or internalization. In such case, use of multiple carbohydrates and a ratiometric analysis allows for discriminating one bacteria from another. Otten *et al.*[31] have documented the feasibility of this approach. Their system, however, is impractical for clinical applications since the bacteria utilized in their study were fluorescently labeled first by biotinylation, followed by direct conjugation with FITC-labelled streptavidin (**Figure 44**). The fluorescently labeled bacteria were then incubated in a 96 well plate bearing different carbohydrates **(Figure 45)**.
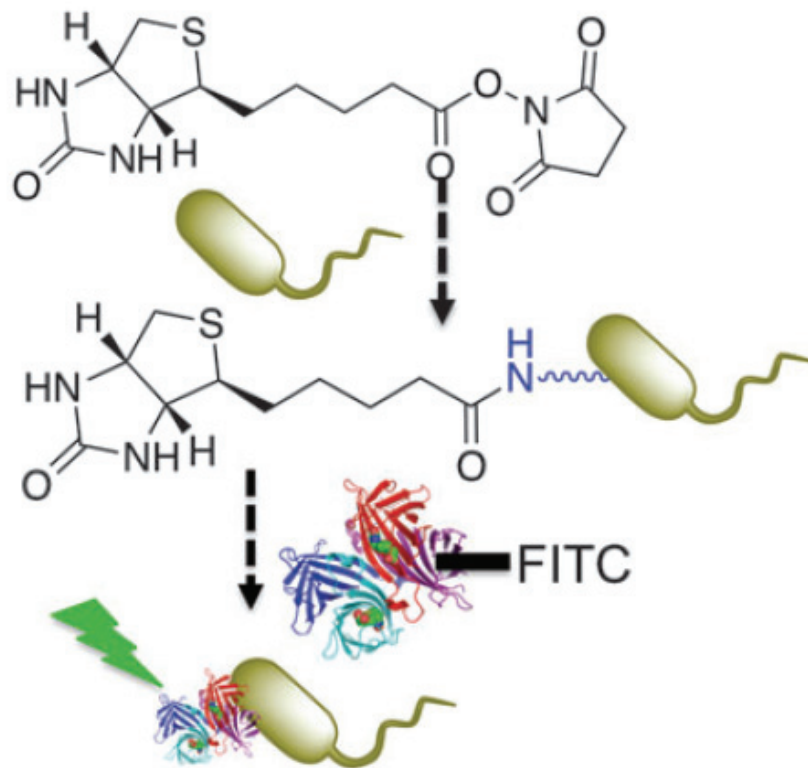

Figure 44. Fluorescent labeling of bacteria with FITC. Reproduced from reference 31 with permission.
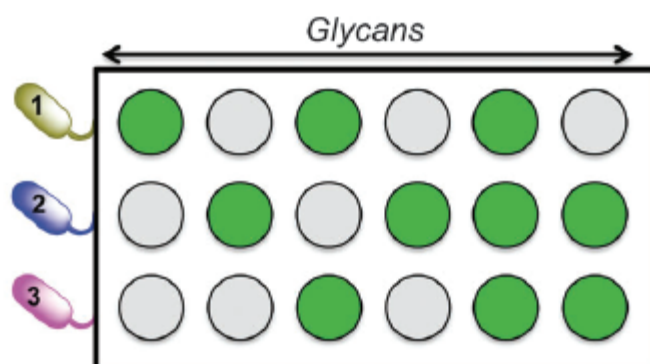
Figure 45. Screening of fluorescently labeled bacteria on a carbohydrate-bearing 96 well plate. Reproduced from reference 31 with permission.

Otten *et al.*[31] were able to correctly identify a strain of *E. coli* with 96% certainty in their system. Despite the great success of this ratiometric method, it is still impractical in clinical settings, as the bacteria must be first fluorescently labeled. It is therefore interesting to develop a rapid, inexpensive method for identification of bacteria.

7.2 Approach toward the Synthesis of Protected Sugar Azides

Triethylene glycol monoazide was synthesized using a modified protocol.[42] First, triethylene glycol monotosylate was synthesized by reaction of triethylene glycol with *p*-tolunesulfonyl chloride in the presence of silver (I) oxide and a catalytic amount of potassium iodide. Then, triethylene glycol monoazide was synthesized by reacting the previously synthesized triethylene glycol monotosylate with sodium azide to yield crude triethylene glycol monoazide (**Figure 46**).
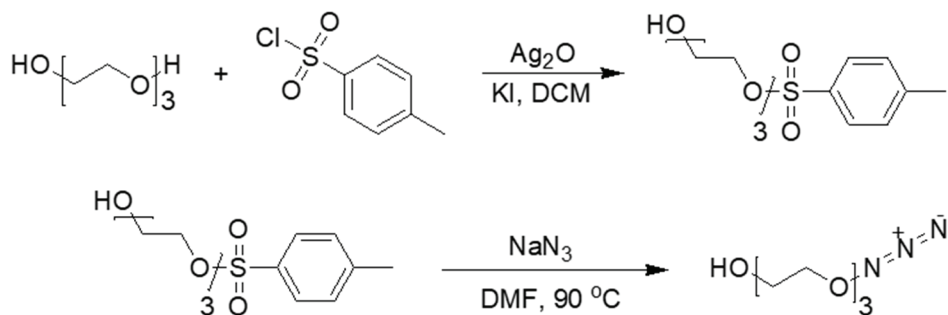
Figure 46. Synthesis of triehtylene glycol monoazide.

Triethylene glycol monoazide will then be reacted with one of three monosaccharides, glucose, galactose, or mannose to yield a sugar conjugated to a terminal azide for future CuAAc chemistry. To accomplish this, each sugar will first be protected by acetylating each alcohol. This will be done by reacting each sugar (**Figure 47**) with acetic anhydride in pyridine. Following this, triethylene glycol monoazide may then be reacted with the protected sugar in boron trifluoride etherate as a lewis acid[42] (**Figure 48**).
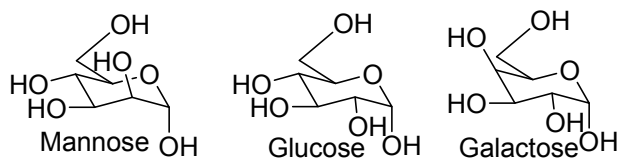

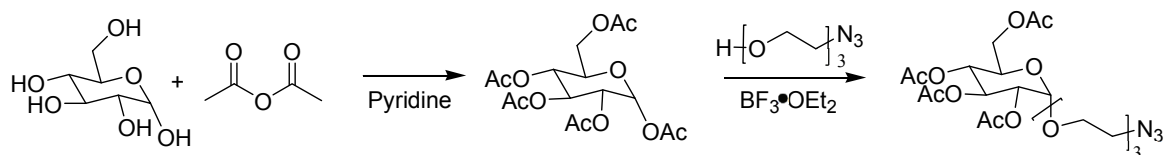Figure 47. Structures of mannose, glucose, and galactose.

Figure 48. Synthetic scheme for protected sugar-azides.

7.3 Approach toward the Synthesis of Fluorescein and Rhodamine B with Terminal Alkynes

Three common and inexpensive fluorophores were chosen: 6-hydroxycoumarin, rhodamine B, and fluorescein (**Figure 49**), which fluoresce blue, red, and green, respectively. Each of these will be conjugated with a terminal alkyne. Rhodamine B and fluorescein will be reacted directly with the terminal alkyne source, propargyl alcohol (**Figures 50 and 51**).
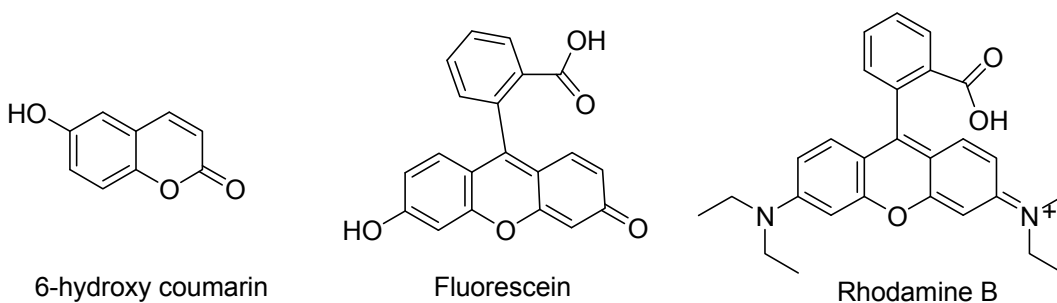

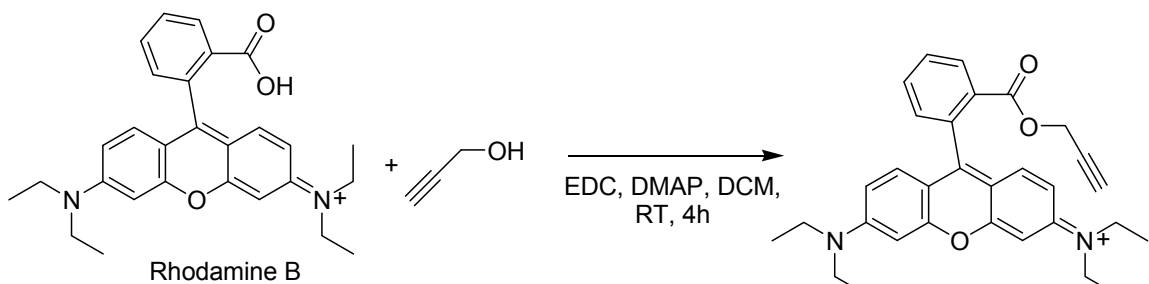Figure 49. Structures of 6-hydroxycoumarin, fluorescein, and rhodamine B.

Figure 50. Synthesis of rhodamine B with a terminal alkyne. Reference 43.
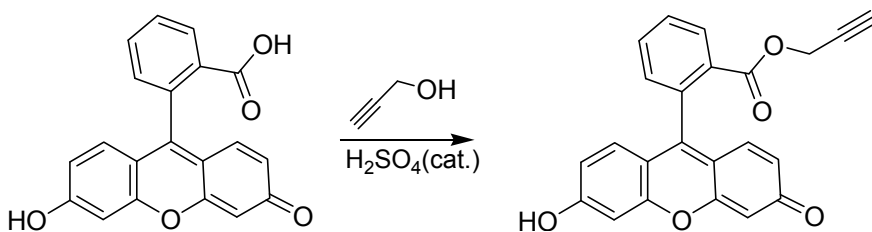

Figure 51. Synthesis of fluorescein with a terminal alkyne.

7.4 Approach toward the Synthesis of 6-hydroxycoumarin with Terminal Alkynes

Prior to reaction with 6-hydroxycoumarin, however, the hydroxyl group from propargyl alcohol must be converted to a good leaving group. This is accomplished by substituting the hydroxyl group with a tosylate[44], as shown in **Figure 52**. After formation of propargyl tosylate the terminal alkyne may be added to 6-hydroxycoumarin, as shown in **Figure 53**.
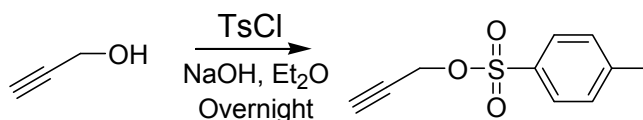
Figure 52. Synthesis of propargyl tosylate. Reference 44.
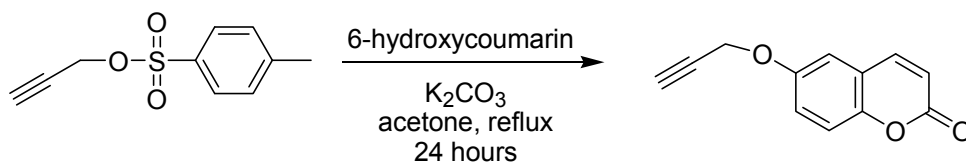
Figure 53. Synthesis of 6-hydroxycoumarin with a terminal alkyne.

This will yield each fluorophore (rhodamine B, fluorescein, and 6-hydroxycoumarin) with a terminal alkyne, and each sugar (mannose, glucose, and galactose) with a terminal azide. CuAAC may then be performed between each azide-alkyne pair as shown in the generic reaction scheme. This will yield three sugar fluorophore conjugates (**Figure 40**) rhodamine B conjugated to galactose, fluorescein conjugated to mannose, and 6-hydroxycoumarin conjugated to glucose.

8. RESULTS

8.1 Synthesis of Triethylene Glycol Monotosylate (Figure 54)

Figure 54. Structure of triethylene glycol monotosylate.

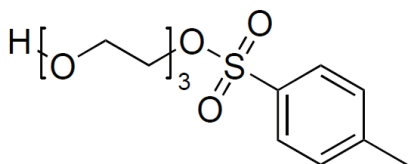To a 100 mL round bottom flask, 0.7582 g of triethylene glycol, 0.1759 g of potassium iodide, 1.7873 g of previously synthesized silver (I) oxide, 1.0168 g of p-toluenesulfonyl chloride, and 50 mL of DCM were added. The reaction was sealed using a rubber septum and reacted overnight at room temperature with stirring, and filtered through a silica gel plug to remove potassium iodide and silver (I) oxide. The filtrate was collected and the silica gel plug was rinsed with a 5 – 10 mL of ethyl acetate to rinse off any remaining product. The filtrates were combined and solvent was removed under vacuum. The crude product was purified using flash chromatography with gradient elution 50 % ethyl acetate / hexanes to 100 % ethyl acetate hexanes. Fractions were collected after TLC analysis. Solvent was removed under vacuum to yield a viscous, transparent oil (1.4491 g, 94.3 % yield): ^{1}H NMR (400 MHz, DMSO-d$_6$): δ 7.79 (d, $J = 8$ Hz, 2H), 7.48 (d, $J = 8$ Hz, 2H), 4.55 (b, 1H, **OH**) 4.11 (m, 2H, **CH$_2$**-SO$_2$), 3.39-3.59 (m, **CH$_2$CH$_2$O**- of PEG backbone), 2.42 (s, 3H, **CH$_3$**) (**Appendix B-1**). ^{13}C NMR (100 MHz, CDCl$_3$): δ 144.88, 132.40, 130.11, 127.61, 72.34, 69.73, 67.89, 60.19, 21.07 (**Appendix B-2**).

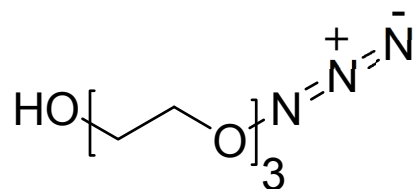**8.2 Synthesis of Triethylene Glycol Monoazide (Figure 55)**

Figure 55. Structure of triethylene glycol monoazide.

In a 50 mL round bottom flask, 1.0 g of triethylene glycol monoazide and 1.0 g of

sodium azide were dissolved in 15 mL DMF and stirred overnight at 90 °C. The reaction

mixture was then filtered to remove excess sodium azide and concentrated under vacuum.

10 mL of DCM was added and washed 2 times with saturated sodium chloride solution,

and then a small amount of water. The organic layer was dried over anhydrous

magnesium sulfate, filtered, and the solvent was removed under vacuum to yield crude

product as a viscous, transparent oil. The TLC and NMR spectrum indicated the

formation of the product. However, further purification is required to obtain the pure

product.

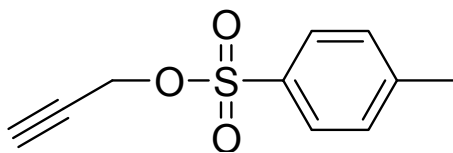**8.3 Synthesis of Propargyl Tosylate (Figure 56)**

Figure 56. Structure of propargyl tosylate.

In a 100 mL round bottom flask, 2.9 mL of propargyl alcohol and 12.5642 g TsCl was stirred in 50 mL of anhydrous diethyl ether until dissolved. The reaction mixture was then stirred on an ice bath and 10.0208 g of sodium hydroxide pellets were added in small portions. After 50 minutes, the reaction was removed from the ice bath and stirred at room temperature overnight. The reaction mixture was then added to 100 mL of ice cold deionized water, leaving behind undissolved sodium hydroxide pellets. The organic layer was removed and the aqueous layer was washed 2 times with 50 mL anhydrous diethyl ether. The organic layers were combined and dried over anhydrous magnesium sulfate and filtered to remove solids. The filtrate was dried under vacuum to yield a straw colored liquid (9.0279 g, 85.4 % yield): ^{1}H NMR (400 MHz, DMSO-d_6): δ 7.71 (d, J = 8 Hz, 2H), 7.27 (d, J = 8 Hz, 2H), 4.60 (d, J = 4 Hz, 2H, **CH$_2$**), 2.45 (t, J = 4Hz, 1H, **CH**), 2.36 (s, 3H, **CH$_3$**) (**Appendix B-3**). ^{13}C NMR (100 MHz, DMSO-d_6): δ 145.22, 132.35, 130.10, 127.70, 80.17, 76.16, 58.21, 21.08 (**Appendix B-4**).

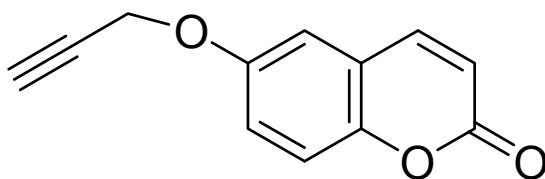## 8.4 Synthesis of Alkyne Terminated 6-hydroxycoumarin (Figure 57)

Figure 57. Structure of alkyne terminated 6-hydroxycoumarin.

To a 25 mL round bottom flask, 120 mg of 6-hydroxycoumarin, 128 mg potassium carbonate, and 12 mL of acetone were added. Then, 0.162 mL of propargyl tosylate was added portionwise. The reaction was then stirred at 50 °C. After 24 hours,

the reaction was filtered to remove solids, and the solvent was removed under vacuum. The crude product was purified via flash chromatography using gradient elution from 100 % hexanes to 100 % ethyl acetate. Fractions were analyzed by TLC, combined, and dried under vacuum to yield an off-white solid (0.064g, 40.1 % yield): ^{1}H NMR (400 MHz, DMSO-d$_6$): δ 8.03 (d, J = 12 Hz, 1H), 7.36 (m, 3H), 6.51 (d, J = 12 Hz, 1H), 4.86 (d, J = 4Hz, 2H, C**H**), 3.60 (t, J = 4 Hz, 1H) (**Appendix B-5**).

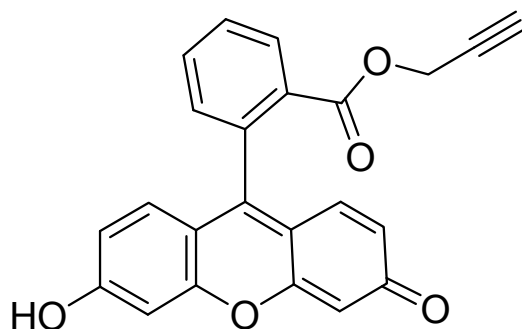## 8.5 Synthesis of Alkyne Terminated Fluorescein (Figure 58)

Figure 58. Structure of alkyne terminated fluorescein.

To a 20 mL round bottom flask, 1.1 g of fluorescein and 10 mL of propargyl alcohol were added. The reaction was stirred on an ice bath while 0.15 mL of concentrated sulfuric acid was added dropwise. The reaction was then heated to 90 °C and reacted overnight. After cooling to room temperature, the reaction was precipitated into 200 mL of deionized water and then washed twice with 50 mL deionized water. The crude product was recovered by vacuum filtration to yield a brown solid. The NMR spectrum indicated the formation of the product. However, further purification is required to obtain the pure product.

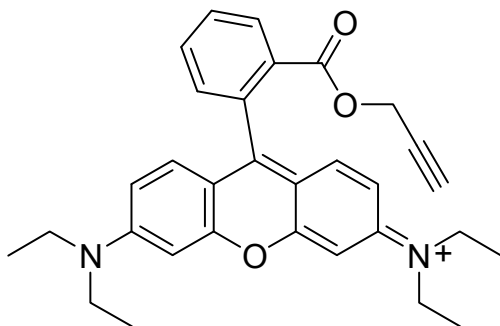**8.6 Synthesis of Alkyne Terminated Rhodamine B (Figure 59)**

Figure 59. Structure of alkyne terminated rhodamine B.

To a 20 mL scintillation vial, 0.2561 g rhodamine B, 34 µL propargyl alcohol, 0.1128 g EDC, 13.1 mg DMAP were added, followed by addition of 3 mL of DCM. This was wrapped in aluminum foil to protect from light. The reaction mixture was stirred at room temperature for 4 hours then washed with 5 mL deionized water. The aqueous layer was then extracted 4 times with 1 mL DCM and all organic layers combined. The combined organic layers were then washed with 5 mL of 0.1 M HCl, 2.5 mL saturated sodium chloride, and dried over anhydrous magnesium sulfate. Solids were filtered off and the solvent removed under vacuum to yield a crude dark violet product. The TLC and NMR spectrum indicated the formation of the product. However, further purification is required to obtain the pure product.

9. FUTURE SYNTHESIS

Figure 60 describes the plan toward the completion of the synthesis. Similar

reactions will be employed for the synthesis of sugar-fluorophore conjugated with

different sugars and/or fluorophore to be used as a probe for the detection of bacteria.
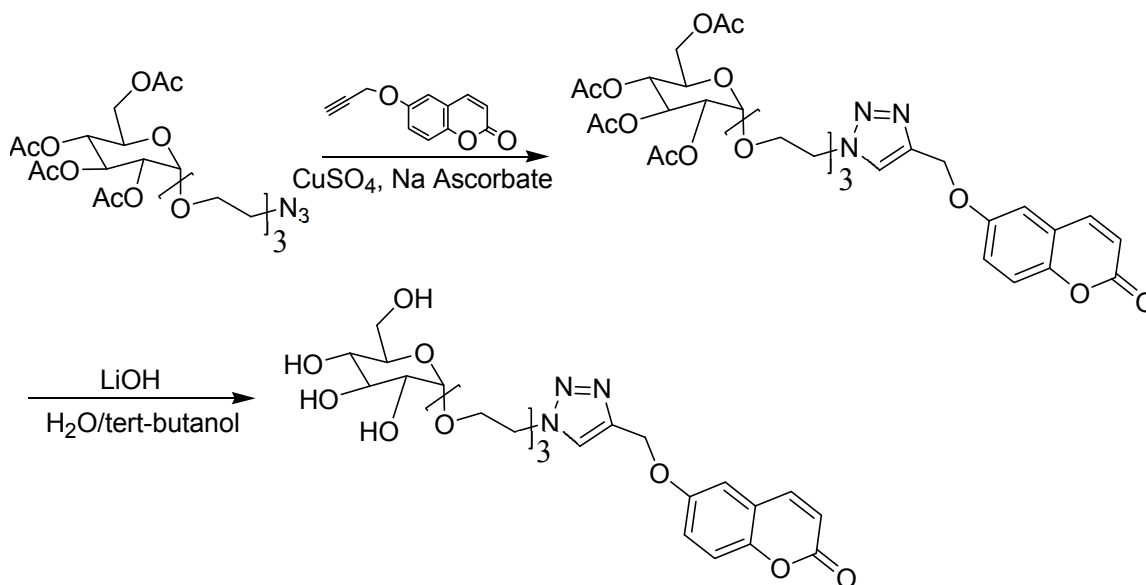

Figure 60. Generic CuAAC reaction between a protected azide terminated sugar and an
alkyne terminated sugar with coumarin and glucose as an example.

10. CONCLUSION

The progress towards the synthesis of sugar-conjugated fluorescent conjugates for bacterial identification are reported. This synthesis will yield a terminal alkyne on each of the three chosen fluorophores and a terminal azide of each of the three sugars. These intermediates will then be coupled by utilizing CuAAc click chemistry to yield the sugar-conjugated fluorescent conjugates. The synthetic steps outlined will be continued, and the effectiveness of these probes in bacterial identification will be evaluated *via* ratiometric analysis in the future.

11. REFERENCES

(1) Kocak, G.; Tuncer, C.; Butun, V., pH-Responsive polymers. *Polym Chem.* **2017,** *8*, 144-176.

(2) Wei, M.; Gao, Y.; Li, X.; Serpe, M., Stimuli-responsive polymers and their applications. *Polym Chem.* **2017,** *8*, 127-143.

(3) Bertrand, O.; Gohy, J.-F., Photo-responsive polymers: synthesis and applications. *Polym Chem.* **2017,** *8* (1), 52-73.

(4) Kim, Y.-J.; Matsunaga, Y., Thermo-responsive polymers and their application as smart biomaterials. *J. Mater. Chem. B.* **2017,** *5*, 4307-4321.

(5) Shieh, Y.-T.; Hu, F.-Z.; Cheng, C.-C., CO2-Switchable Multi-Stimuli-Responsive Polymer Nanoparticle Dispersion. *ACS Appl. Nano Mater.* **2018,** *1*, 384-393.

(6) Holme, M. N.; Fedotenko, I. A.; Abegg, D.; Althaus, J.; Babel, L.; Favarger, F.; Reiter, R.; Tanasescu, R.; Zaffalon, P. L.; Ziegler, A.; Müller, B.; Saxer, T.; Zumbuehl, A., Shear-stress sensitive lenticular vesicles for targeted drug delivery. *Nat Nanotechnol.* **2012,** *7*, 536-43.

(7) Korin, N.; Kanapathipillai, M.; Matthews, B. D.; Crescente, M.; Brill, A.; Mammoto, T.; Ghosh, K.; Jurek, S.; Bencherif, S. A.; Bhatta, D.; Coskun, A. U.; Feldman, C. L.; Wagner, D. D.; Ingber, D. E., Shear-activated nanotherapeutics for drug targeting to obstructed blood vessels. *Science.* **2012,** *337*, 738-42.

(8) Korin, N.; Gounis, M. J.; Wakhloo, A. K.; Ingber, D. E., Targeted drug delivery to flow-obstructed blood vessels using mechanically activated nanotherapeutics. *JAMA Neurol.* **2015,** *72*, 119-22.

(9) Kwak, B. R.; Bäck, M.; Bochaton-Piallat, M. L.; Caligiuri, G.; Daemen, M. J.; Davies, P. F.; Hoefer, I. E.; Holvoet, P.; Jo, H.; Krams, R.; Lehoux, S.; Monaco, C.; Steffens, S.; Virmani, R.; Weber, C.; Wentzel, J. J.; Evans, P. C., Biomechanical factors in atherosclerosis: mechanisms and clinical implications. *Eur. Heart J.* **2014,** *35*, 3013-20.

(10) Natsume, T.; Yoshimoto, M., Mechanosensitive liposomes as artificial chaperones for shear-driven acceleration of enzyme-catalyzed reaction. *ACS Appl. Mater. Interfaces* **2014,** *6*, 3671-9.

(11) Takeda, K.; Yamasaki, Y.; Dirisala, A.; Ikeda, S.; Tockary, T.; Toh, K.; Osada, K.; Kataoka, K., Effect of shear stress on structure and function of polyplex micelles from poly(ethylene glycol)-poly(L-lysine) block copolymers as systemic gene delivery carrier. *Biomaterials* **2017,** *126*, 31-38.

(12) Chen, H.; Kim, S.; Li, L.; Wang, S.; Park, K.; Cheng, J.-X., Release of hydrophobic molecules from polymer micelles into cell membranes revealed by Forster   resonance energy transfer imaging. *Proc. Natl. Acad. Sci. U.S.A.* **2008,** *105*, 6596-6601.

(13) Chen, H.; Kim, S.; He, W.; Wang, H.; Low, P.; Park, K.; Cheng, J.-X., Fast Release of Lipophilic Agents from Circulating PEG-PDLLA Micelles Revealed by in Vivo Fo¨rster Resonance Energy Transfer   Imaging. *Langmuir* **2008,** *24*, 5213-5217.

(14) Brown, R., Spontaneous lipid transfer between organized lipid assemblies. *Biochim. Biophys. Acta.* **1992,** *113*, 375-389.

(15) Larsen, M. B.; Boydston, A. J., Successive Mechanochemical Activation and Small Molecule Release in an Elastomeric Material. *J. Am. Chem. Soc.* **2014,** *136*, 1276-1279.

(16) Chemistry LibreTexts™. Fluorescence Resonance Energy Transfer. https://chem.libretexts.org/Textbook_Maps/Physical_and_Theoretical_Chemistry_ Textbook_Maps/Supplemental_Modules_(Physical_and_Theoretical_Chemistry)/F undamentals/Fluorescence_Resonance_Energy_Transfer (accessed July 1, 2018).

(17) Jenkins, A.; Jones, R.; Moad, G., Terminology for reversible-deactivation radical polymerization previously called "controlled" radical or "living" radical polymerization (IUPAC Recommendations 2010). *Pure Appl. Chem.* **2010,** *82*, 483-491.

(18) Keddie, D., A guide to the synthesis of block copolymers using reversible-addition fragmentation chain transfer   (RAFT) polymerization. *Chem. Soc. Rev.* **2013,** *43*, 496-505.

(19) Keddie, D.; Moad, G.; Rizzardo, E.; Thang, S., RAFT Agent Design and Synthesis. *Macromolecules* **2012,** *45*, 5321-5342.

(20) Pound, G.; Augesse, F.; McLeary, J.; Lange, R.; Klumperman, B., Xanthate-Mediated Copolymerization of Vinyl Monomers for Amphiphilic and Double-Hydrophilic Block Copolymers with   Poly(ethylene glycol). *Macromolecules* **2007,** *40*, 8861-8871.

(21) Willersinn, J.; Drechsler, M.; Antonietti, M.; Schmidt, B., Organized Polymeric Submicron Particles via Self-Assembly and Cross-Linking of Double Hydrophilic Poly(ethyleneoxide) *b* poly(*N* vinylpyrrolidone) in Aqueous Solution. *Macromolecules* **2016,** *49*, 5331–5341.

(22) Mu, B.; Li, X.; Chen, K.; Zeng, Y.; Fang, J.; Chen, D., Controlled Synthesis and Microstructure Tuning of PEG-Containing Side-Chain Discotic Liquid Crystalline Block Copolymers via RAFT   Polymerization. *J. Polym. Sci. A Polym. Chem.* **2017,** *55*, 2544-2553.

(23) Zhao, H.; Jiang, J.; Lim, Y.; Kim, S.-H.; Piao, L., A novel self-seeding polyol synthesis of Ag nanowires using mPEG-b-PVP diblock copolymer. *RSC Adv.* **2014,** *4*, 41927-41933.

(24) Etchenausia, L.; Khoukh, A.; Lejeune, E.; Save, M., RAFT/MADIX emulsion copolymerization of vinyl acetate and N-vinylcaprolactam: towards waterborne physically crosslinked thermoresponsive particles. *Polym. Chem.* **2017,** *8*, 2244-2256.

(25) Etchenausia, L.; Rodrigues, A.; Harrisson, S.; Lejeune, E.; Save, M., RAFT Copolymerization of Vinyl Acetate and N   Vinylcaprolactam: Kinetics, Control, Copolymer Composition, and Thermoresponsive   Self-Assembly. *Macromolecules* **2016,** *49*, 6799-6809.

(26) Stenzel, M.; Cummins, L.; Roberts, G. E.; Davis, T.; Vana, P., Xanthate Mediated Living Polymerization of Vinyl Acetate: A Systematic Variation in MADIX/RAFT   Agent Structure. *Macromol. Chem. Phys.* **2003,** *204*, 1160-1168.

(27) BASF, Solubility Enhancement with BASF Pharma Polymers. In *Solubilizer Compendium* [Online] Reintjes, T., Ed. BASF SE: Lampertheim, Germany, 2011; p. 130.

(28) Harrisson, S.; Liu, X.; Ollagnier, J.-N.; Coutelier, O.; Marty, J.-D.; Destarac, M., RAFT Polymerization of Vinyl Esters: Synthesis and Applications. *Polymers* **2014,** *6*, 1437-1488.

(29) Perrier, S., 50th Anniversary Perspective: RAFT Polymerization-A User Guide. *Macromolecules* **2017,** *50*, 7433-7477.

(30) Kolb, H. C.; Finn, M. G.; Sharpless, K. B. Click Chemistry: Diverse Chemical Function from a Few Good Reactions. *Angew. Chem., Int. Ed.* **2001**, *40*, 2004-2021

(31) Otten, L.; Fullam, E.; Gibson, M., Discrimination between bacterial species by ratiometric analysis of their carbohydrate binding profile. *Mol Biosyst* **2016,** *12*, 341-344.

(32) Disney, M.; Seeberger, P., The Use of Carbohydrate Microarrays to Study Carbohydrate-Cell Interactions and to Detect Pathogens. *Chem. Biol.* **2004,** *11*, 1701-1707.

(33) Nimrichter, L.; Gargir, A.; Gortler, M.; Altstock, R.; Shtevi, A.; Oori, W.; Fire, E.; Dotan, N.; Schnaar, R., Intact cell adhesion to glycan microarrays. *Glycobiology* **2004,** *14*, 197-203.

(34) Costerton, J.; Post, J.; Ehrlich, G.; Hu, F.; Kreft, R.; Nistico, L.; Kathju, S.; Stoodley, P.; Hall-Stoodley, L.; Maale, G.; James, G.; Sotereanos, N.; DeMeo, P., New methods for the detection of orthopedic and other biofilm infections. *FEMS Immunol. Med. Microbiol.* **2011,** *61*, 133-140.

(35) Tan, S.; Chew, S.; Tan, S.; Givskov, M.; Yang, L., Emerging frontiers in detection and control of bacterial biofilms. *Curr. Opin. Biotechnol.* **2014,** *26*, 1-6.

(36) Pasquaroli, S.; Zandri, G.; Vignaroli, C.; Vuotto, C.; Donelli, G.; Biavasco, F., Antibiotic pressure can induce the viable but non-culturable state in Staphylococcus aureus growing in biofilms. *J. Antimicrob. Chemother.* **2013,** *68*, 1812-7.

(37) Doughty, E. L.; Sergeant, M. J.; Adetifa, I.; Antonio, M.; Pallen, M. J., Culture-independent detection and characterisation of Mycobacterium tuberculosis and M. africanum in sputum samples using shotgun metagenomics on a benchtop sequencer. *PeerJ* **2014,** *2*.

(38) Halachev, M. R.; Chan, J. Z.; Constantinidou, C. I.; Cumley, N.; Bradley, C.; Smith-Banks, M.; Oppenheim, B.; Pallen, M. J., Genomic epidemiology of a protracted hospital outbreak caused by multidrug-resistant Acinetobacter baumannii in Birmingham, England. *Genome Med.* **2014,** *6*, 70.

(39) Mahou, R.; Wandrey, C., Versatile Route to Synthesize heterobifunctional Poly(ethylene glycol) of Variable Functionality for Subsequent Pegylation. *Polymers* **2012,** *4*, 561-589.

(40) Ning, X.; Lee, S.; Wang, Z.; Kim, D.; Stubblefield, B.; Gilbert, E.; Murthy, N., Maltodextrin-based imaging probes detect bacteria in vivo with high sensitivity and specificity. *Nat. Mater.* **2011,** *10,* 602-607.

(41) Chen, L.-Q.; Hou, B.-H.; Lalonde, S.; Takanaga, H.; Hartung, M. L.; Qu, X.-Q.; Guo, W.-J.; Kim, J.-G.; Underwood, W.; Chaudhuri, B.; Chermak, D.; Antony, G.; White, F. F.; Somerville, S. C.; Mudgett, M. B.; Frommer, W. B., Sugar transporters for intercellular exchange and nutrition of pathogens. *Nature* **2010,** *468*, 527.

(42) Wu, B.; Wei, N.; Thon, V.; Wei, M.; Yu, Z.; Xu, Y.; Chen, X.; Liu, J.; Wang, P.; Li, T., Facile chemoenzymatic synthesis of biotinylated heparosan hexasaccharide. *Org. Biomol. Chem.* **2015,** *13*, 5098-5101.

(43) Chen, X.; Wu, Q.; Henschke, L.; Weber, G.; Weil, T., An efficient and versatile approach for the preparation of a rhodamine B ester bioprobe library. *Dyes Pigm.* **2012,** *94*, 296-303.

(44) Zhang, Q.; Ren, H.; Baker, G., An economical and safe procedure to synthesize 2-hydroxy-4-pentynoic acid: A precursor towards 'clickable' biodegradable polylactide. *Beilstein J. Org. Chem.* **2014,** *10*, 1365-1371.
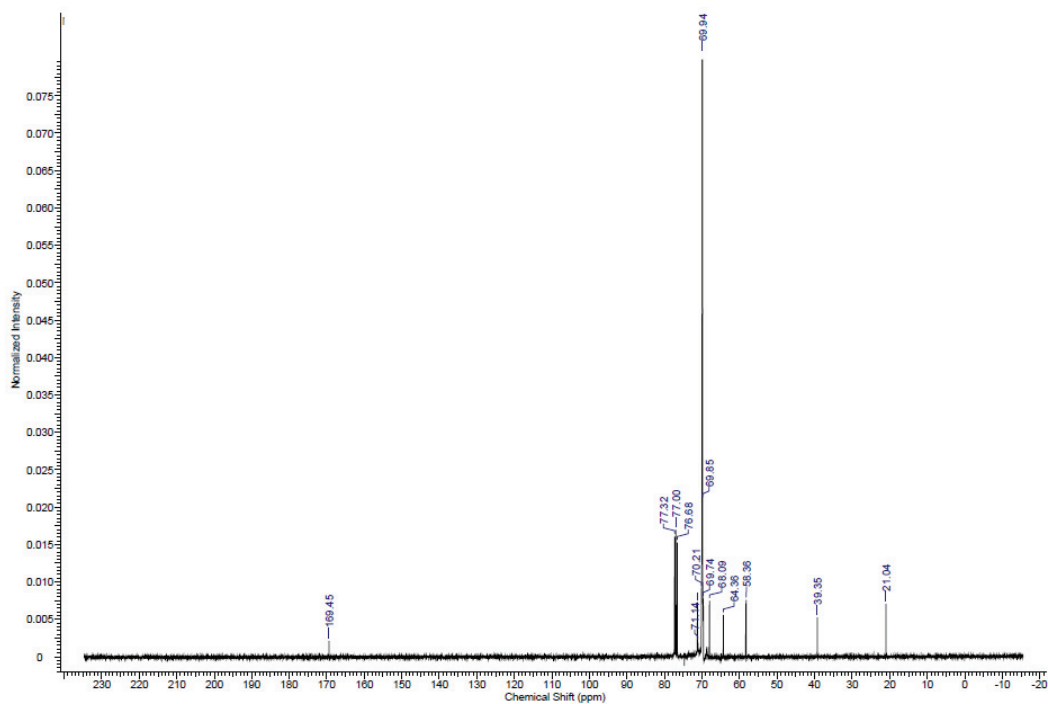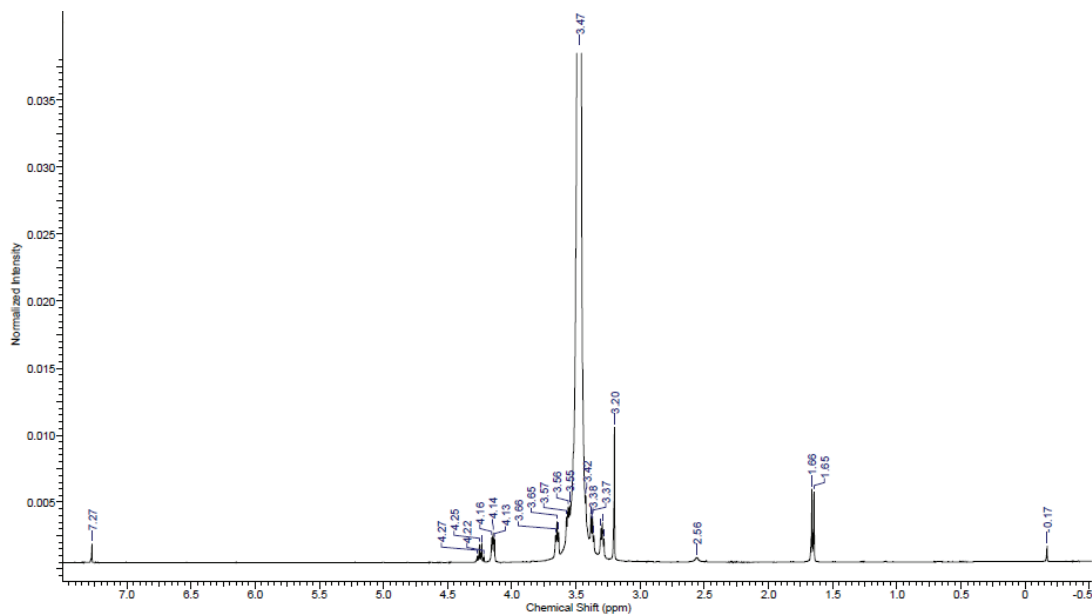
Appendix A: NMRs for Shear Force Responsive Polymers
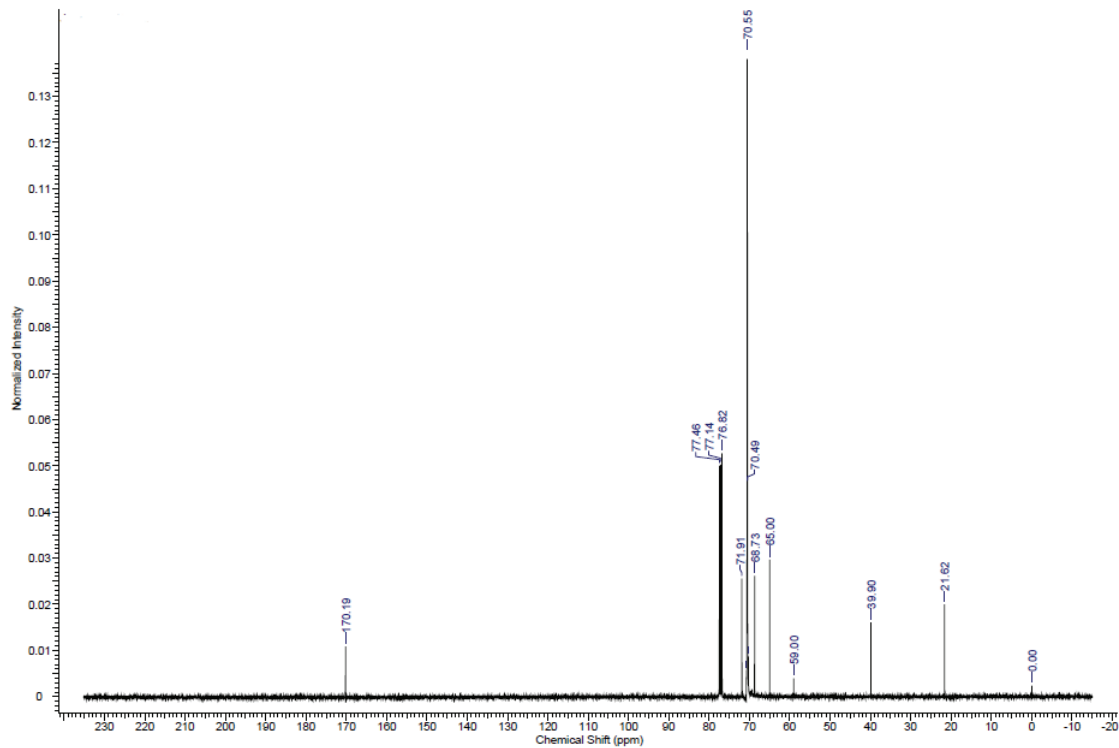
Appendix A-1. ^{13}C NMR spectrum of monomethoxy poly(ethylene glycol) 2,000-2-bromoethyl ester (**1A**) in CDCl$_3$.
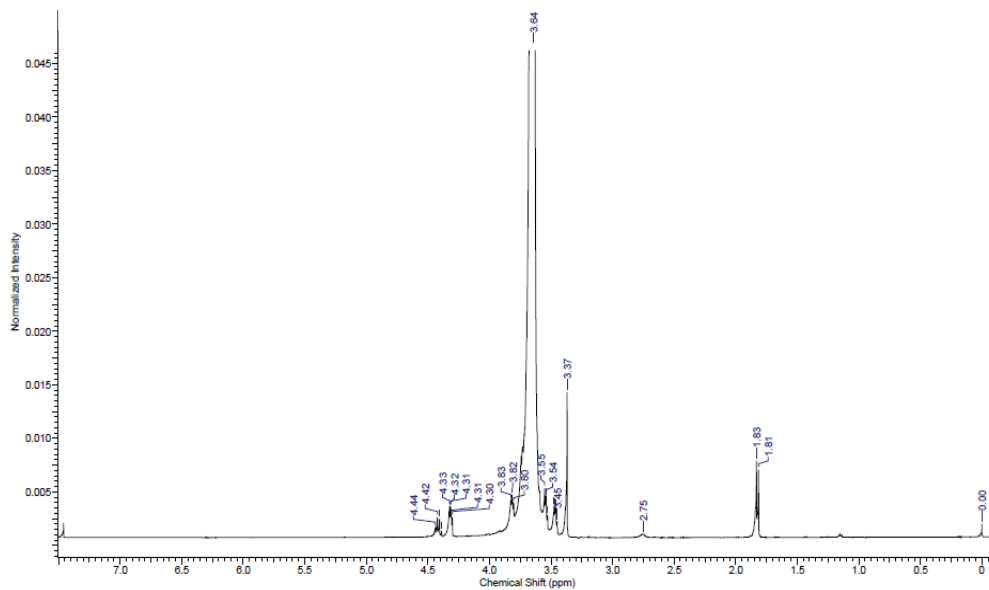
Appendix A-2. ^{1}H NMR spectrum of of monomethoxy poly(ethylene glycol) 4,000-2-bromoethyl ester (**2A**) in CDCl$_3$.

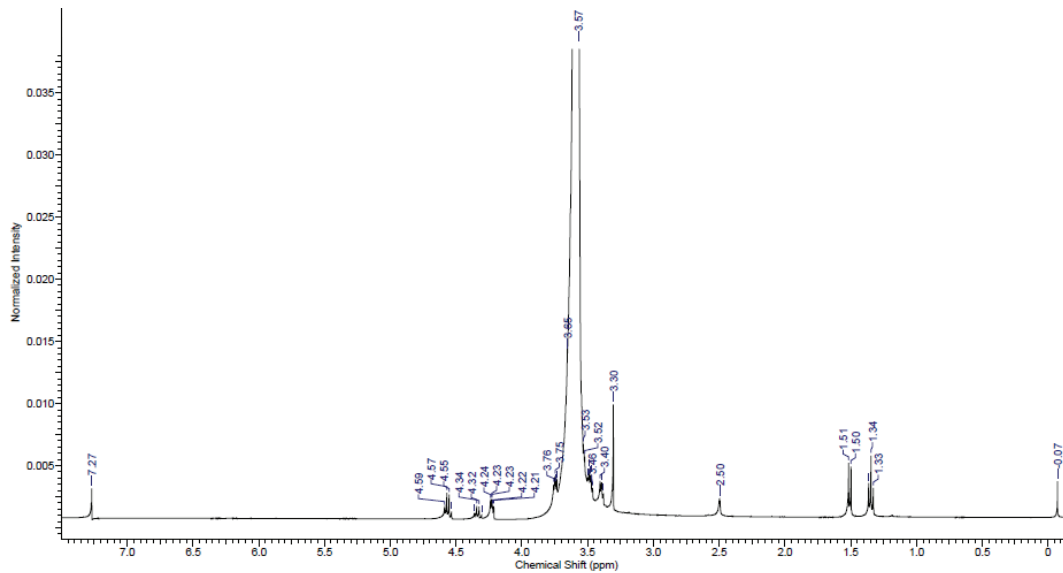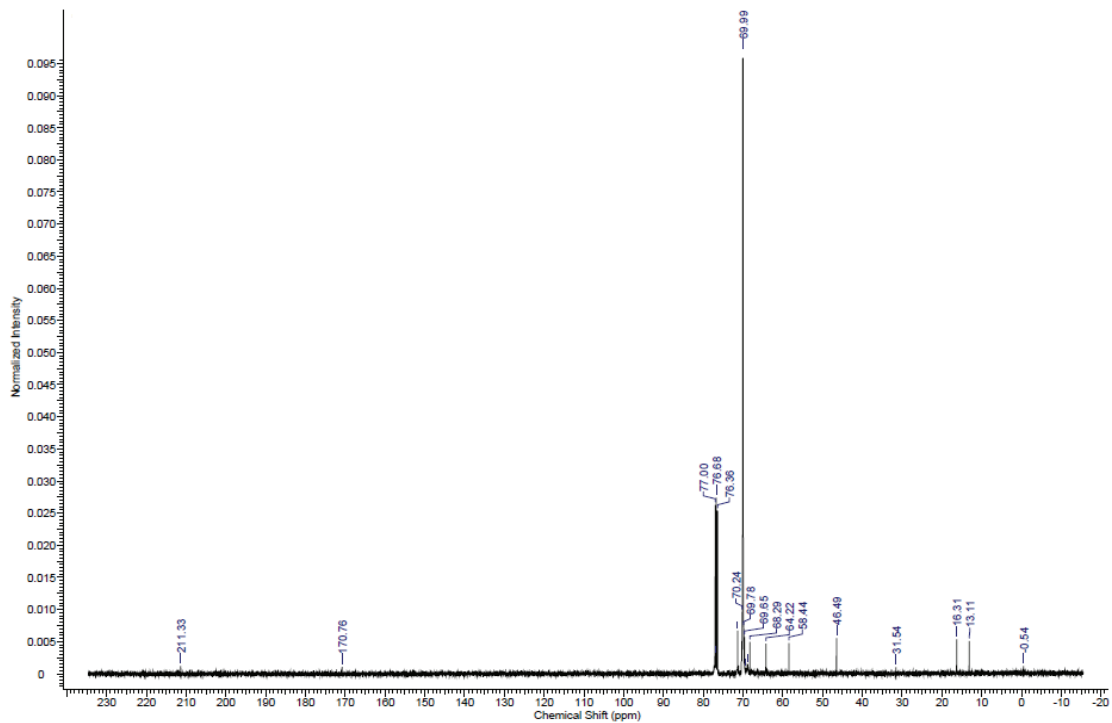Appendix A-3. ^{13}C NMR spectrum of monomethoxy poly(ethylene glycol) 4,000-2-bromoethyl ester (**2A**) in CDCl$_3$.

Appendix A-4. ^{1}H NMR spectrum of monomethoxy poly(ethylene glycol) 5,000-2-bromoethyl ester (**3A**) in CDCl$_3$.
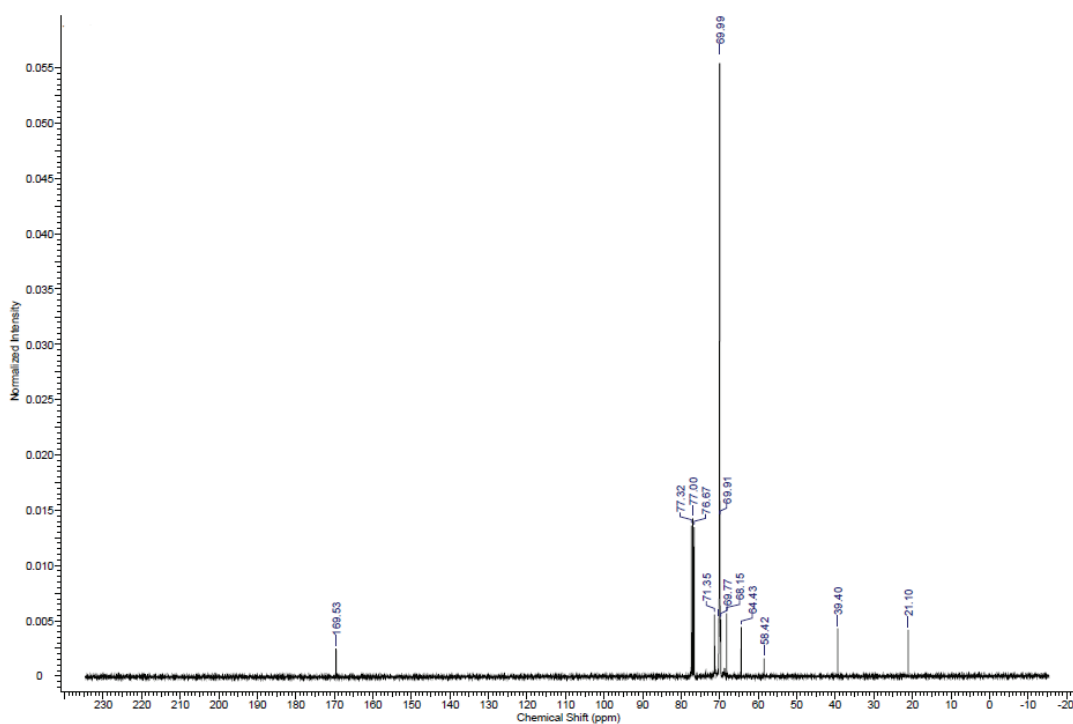
Appendix A-5. ^{13}C NMR spectrum of monomethoxy poly(ethylene glycol) 5,000-2-bromoethyl ester (**3A**) in CDCl$_3$.
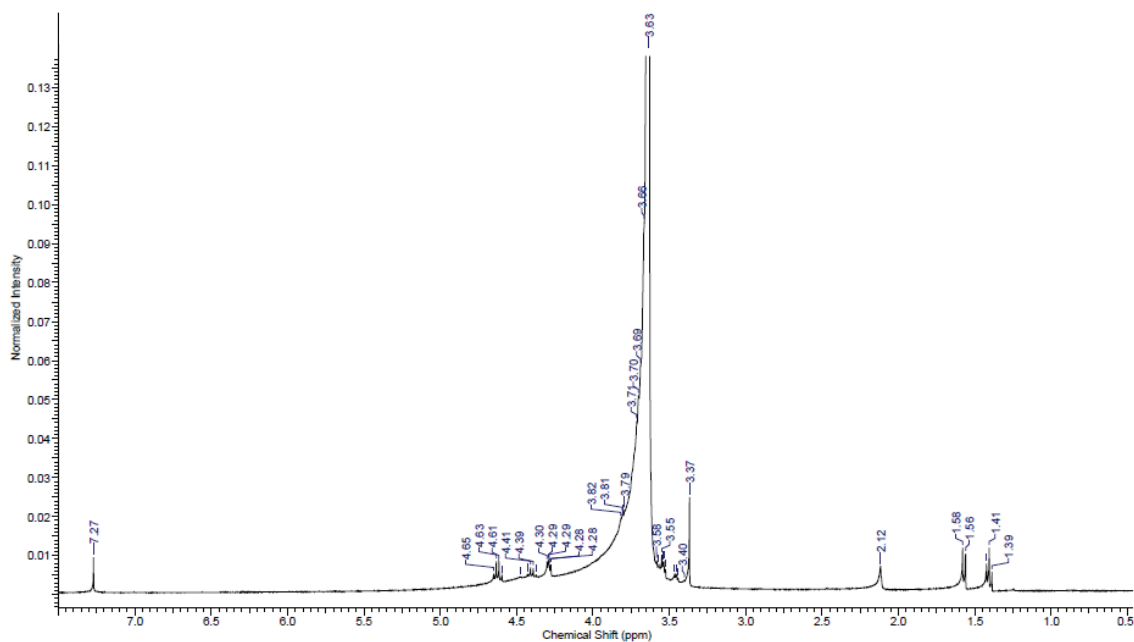
Appendix A-6. ^{1}H NMR spectrum of *S*-2-(monomethoxy poly(ethylene glycol) 2,000 propionate)-(*O*-ethyl xanthate) (**1B**) in CDCl$_3$.
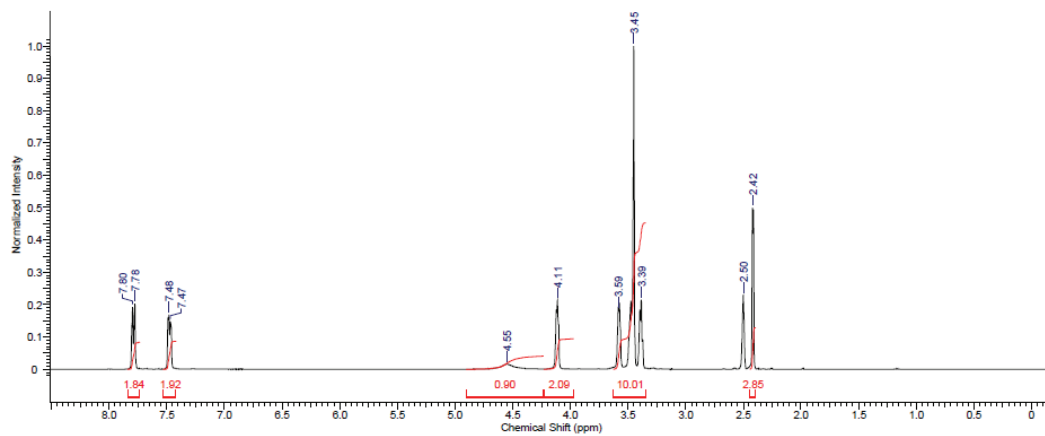

Appendix A-7. ^{1}H NMR spectrum of *S*-2-(monomethoxy poly(ethylene glycol) 5,000 propionate)-(*O*-ethyl xanthate) (**3B**) in CDCl$_3$.
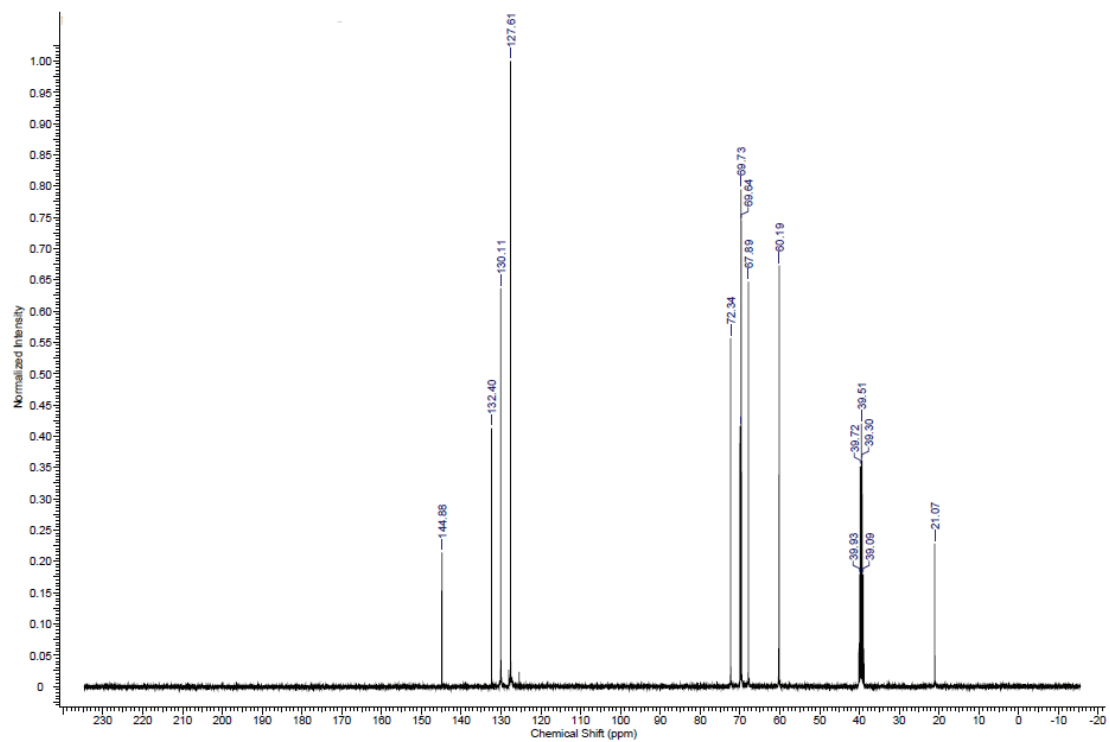
Appendix A-8. ^{13}C NMR spectrum of *S*-2-(monomethoxy poly(ethylene glycol) 5,000 propionate)-(*O*-ethyl xanthate) (**3B**) in CDCl$_3$.
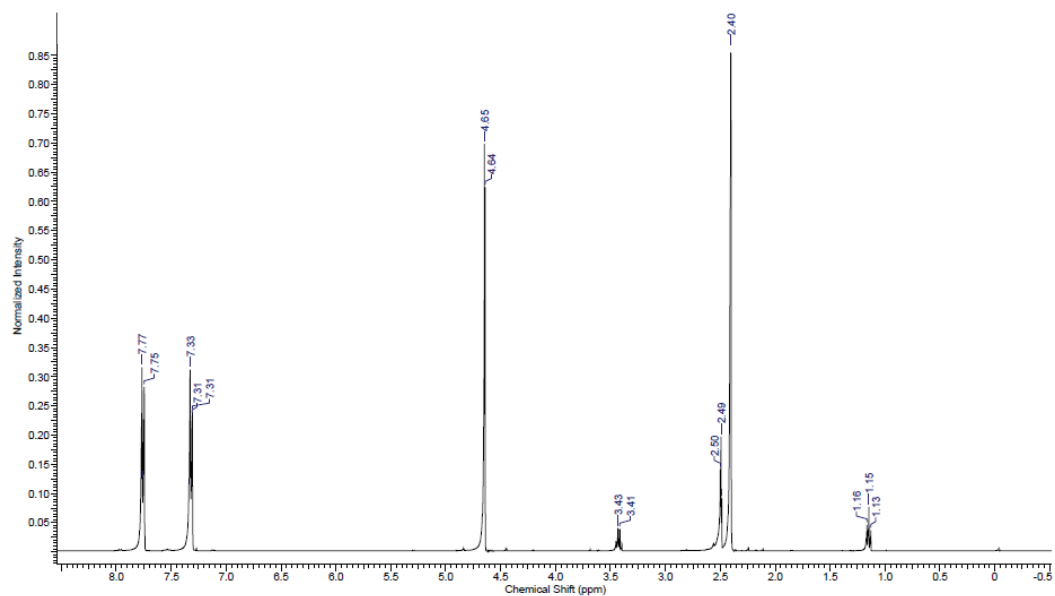
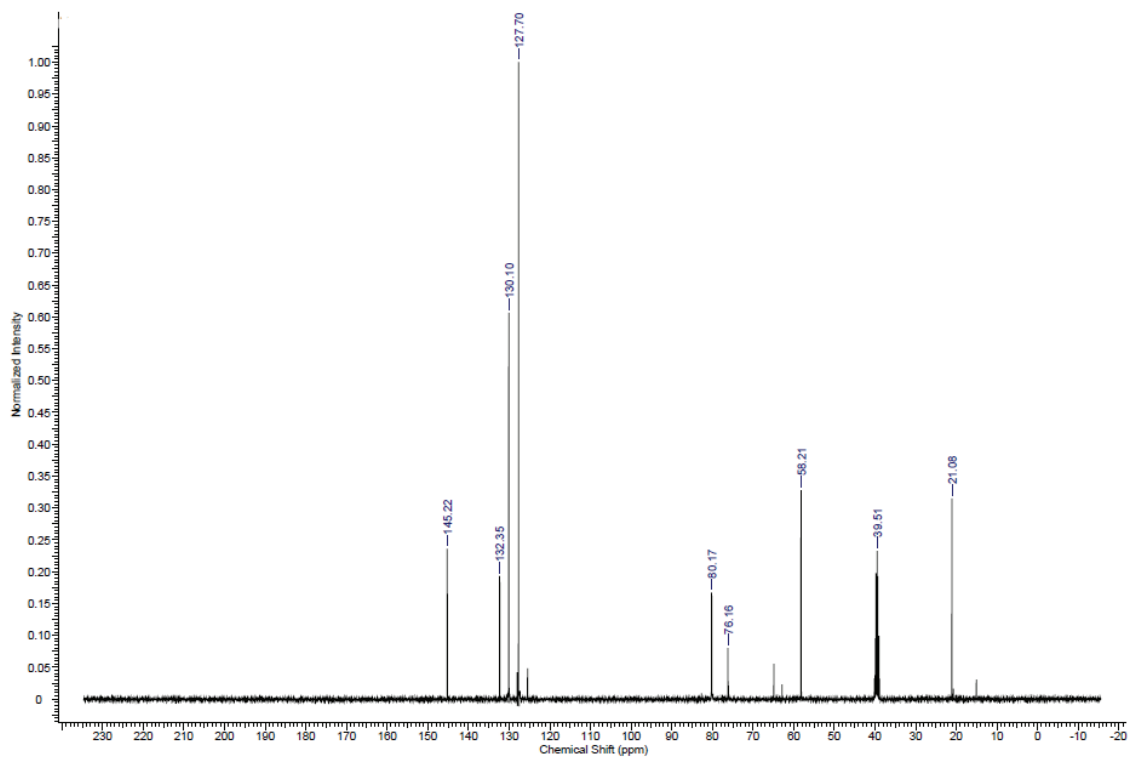## Appendix B: NMRs for Sugar-fluorophore Conjugates.

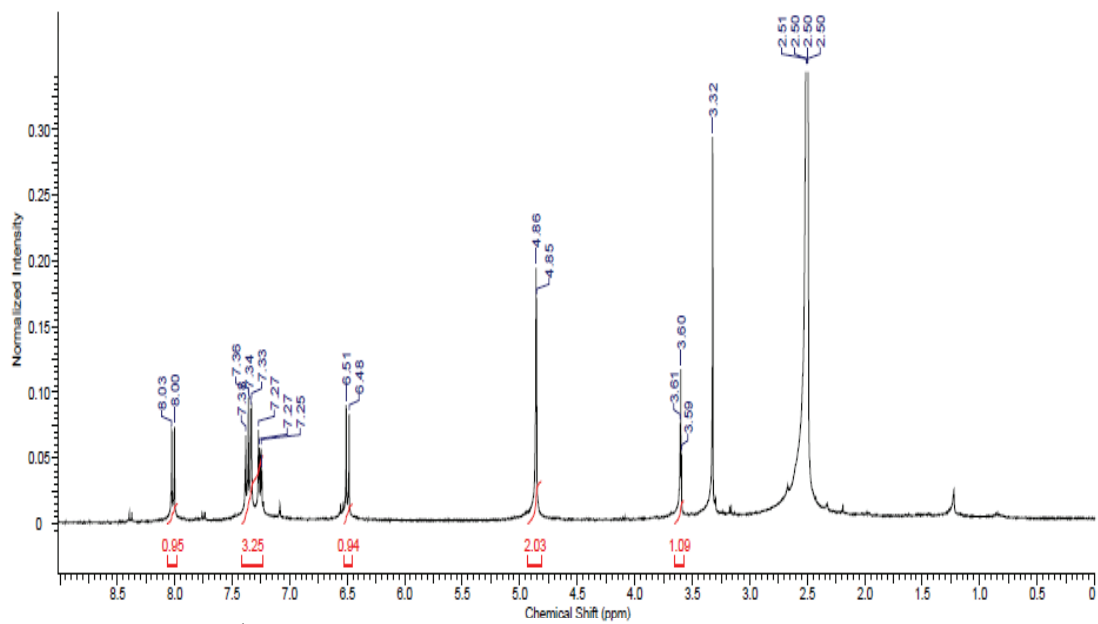Appendix B-1. ^{1}H NMR spectrum of triethylene glycol monotosylate in DMSO-*d*$_6$.

Appendix B-2. ^{13}C NMR spectrum of triethylene glycol monotosylate in DMSO-d_6.

Appendix B-3. ^{1}H NMR spectrum of propargyl tosylate in CDCl$_3$.

Appendix B-4. ^{13}C NMR spectrum of propargyl tosylate in DMSO-d_6.

Appendix B-5. ^{1}H NMR spectrum of alkyne terminated coumarin in DMSO-d_6.